Smart Design of Highly Luminescent Octupolar Mesogenic Tetra styryl-alkynyl Bipyrimidine-Based Chromophores Presenting Non-Linear Optical Properties

Deniz B Vardar, Stephania Abdallah, Rana Mhanna, Prescillia Nicolas, Ahmet Dok, Yovan S de Coene, Stijn Van Cleuvenbergen, Olivier Jeannin, Jean-Pierre Malval, Thierry Verbiest, et al.

Smart Design of Highly Luminescent Octupolar Mesogenic Tetra styryl-alkynyl Bipyrimidine-Based Chromophores Presenting Non-Linear Optical Properties

Deniz Vardar, [a] Stephania Abdallah, [b] Rana Mhanna, [b] Prescillia Nicolas, [c] Ahmet Dok, [d] Yovan de Coene, [d] Stijn Van Cleuvenbergen, [d] Olivier Jeannin, [c] Jean-Pierre Malval, [b] Thierry Verbiest, [d] Koen Clays, [d] Nathalie Bellec, [c] Belkis Bilgin-Eran, [a] Franck Camerel,*[c] and Huriye Akdas-Kiliç*[a,c]

[a] D. Vardar, Pr. B. Bilgin-Eran, Pr. H. Akdas-Kiliç
Department of Chemistry
Yildiz Technical University
Istanbul, Turkey
E-mail: hakdas@yildiz.edu.tr

[b] S. Abdallah, R. Mhanna, Pr. Jean-Pierre Malval
Institut de Science des Matériaux de Mulhouse CNRS-UMR 7361
Université de Haute Alsace
Mulhouse, France

[c] P. Nicolas, Dr. N. Bellec, Dr. O. Jeannin, Dr. F. Camerel
Institut des Sciences Chimiques de Rennes CNRS UMR
Université de Rennes
Rennes, France
E-mail : franck.camerel@univ-rennes.fr

[d] A. Dok, Dr. Y. de Coene, Pr. S. Van Cleuvenbergen, Pr. T. Verbiest, Pr. K. Clays
Department of Chemistry
Katholieke Universiteit Leuven
Leuven, Belgium

Keywords: Bipyrimidine, Liquid Crystal, Luminescence, Two-Photon absorption, Nonlinear Optic

Abstract:

The research investigations reported in this paper focuses on the influence of rational design on the photophysical properties of new all-organic multifunctional chromophores. Nonlinear optical (NLO) behavior, optical properties and mesogenicity of several new π-conjugated octupolar chromophores, presenting alkoxy styryl-alkynyl donor groups carrying aliphatic achiral and chiral chains in the 3,4 / 3,5 / 2,4 position, connected to electron-accepting 2,2-bipyrimidine cores are investigated by various techniques (light-transmission measurements, polarized-light optical microscopy, differential scanning calorimetry measurements, two-photon excited fluorescence and Hyper Rayleigh Scattering). The mesogenic properties were investigated depending on the position of the alkoxy chain and the 3,4 derivatives were found to exhibit liquid-crystal with the formation columnar phases over large temperature ranges which were confirmed by small-angle X-ray scattering analysis. All the molecules exhibit exceptional high fluorescence quantum yields values around 80 % and excellent nonlinear optical properties.

Introduction

In the last decade, the development of smart soft materials has been subject of intensive research for various critical applications in advanced technologies [1]. Recent successful examples have been demonstrated in a vast variety of fields such as colloids, foams, liquid crystals (LCs), gels, polymers, and active matter [2]. Among the soft materials, Liquid Crystals (LCs) represents one of the most attractive soft matter systems [3]. LCs, because of their responsive and adaptive properties along with their relatively easy alignment and reorientation, are primarily known for their industrial applications in LC display (LCD) devices for visualizing information [4]. However, since they can achieve intriguing and programmable hierarchical superstructures through molecular self-assembly, the use of LCs has been demonstrated in different areas of material technologies, biological and biomedical science, and nanotechnologies [5].

A way to enrich the functions of liquid crystals is to design the mesogens units in a π-conjugated fashion by molecular engineering. Indeed, this first level of smart design of π-conjugated materials with self-organizing properties have been increasingly applied in the field of advanced platforms for new multifunctional materials [6]. The development of versatile synthetic methodology allows the synthesis of extended conjugated organic molecules based on the donor-bridge-acceptor design that displays intramolecular charge transfer [7] (ICT) upon excitation, which can lead to photophysical, electrochemical and magnetic properties. The electrons delocalization along the dipolar conjugated backbones result in amplification of luminescence and an electronic nonlinearity, which will give second and third order nonlinear optical (NLO) behaviour. In order to optimize NLO properties, a second level of smart design is to add dimensionality to these building blocks by using octupolar conjugated molecules instead of dipolar, because they exhibit a better efficiency/transparency by stabilizing a macroscopic non-centrosymmetric order which is essential to obtain second-order NLO materials [8]. In particular, second-order NLO materials have a variety of applications ranging from medical therapies to semi-conductor manufacturing as well as information technologies [9].
The fine-tuning and optimization of compounds for a given task in photonics require a deep understanding of the influence of structural variations on the optical properties of interest [10]. Recently, a new class of three-dimensional NLO-phores with D_{2d} symmetry based on donor-substituted styryl bipyrimidine cores has been investigated [11]. Such derivatives exhibit interesting mesogenic, fluorescence and fluoro-solvatochromic properties as well as large cubic and quadratic NLO responses (second harmonic generation SHG and two-photon absorption TPA), which can be tuned by the nature of the substituents within the styryl fragments [12]. In the present work, the synthesis and complete physicochemical characterization (including linear and nonlinear optical, mesomorphic, thermal, structural) of new multifunctional chromophores are described. A series of octupolar four-branched compounds incorporating a bipyrimidine (BPM) chelating group as an electron-deficient core (Scheme 1) and four divergent lipophilic styryl-alkynyl fragments. The mesogenic and optical properties such as absorption, emission, or NLO behaviors are studied depending on the nature of the alkoxy chain and their substitution pattern on these fragments.

Results and Discussion

Synthesis and Characterization. Synthetic pathways previously reported in the literature were used to obtain the new bipyrimidine based targeted compounds **6a-f** depicted in scheme 1 [13]. The synthesis of 4,4',6,6'-Tetramethyl-2,2'-bipyrimidine **1** was realized via Ullman-type coupling according to previously reported procedures by a nickel-catalyzed self-coupling reaction of commercially available 2-chloro-4,6-dimethylpyrimidine in the presence of nickel chloride, triphenylphosphine and zinc in DMF at 50°C and in an inert atmosphere [14]. The alkoxy-substituted benzaldehyde **2a-f** functionalized in 2,5, 3,5 and 3,4 positions were directly prepared from the corresponding dihydroxybenzaldehyde by Williamson ether alkylation reaction [15] with the corresponding n-alkyl bromide or the (S)-1-bromo-3,7-dimethyloctane prepared by reduction of commercially available (S)-(-)-β-citronellol followed by bromination with concentrated HBr/H_2SO_4 acid [16]. Then, the alkoxy-substituted benzaldehydes **2a-f** were converted into dibromo vinylic derivatives **3a-f** by the Corey-Fuchs procedure and transformed by dehydrohalogenation into the terminal alkyne derivatives **3a-f** by treatment with Butyllithium [17] which was further converted by a second Sonogashira cross-coupling with 4-bromobenzaldehyde into the mesogenic promoters **5a-f** via Copper-Free Sonogashira Coupling Reaction [18]. The final step of synthesis, to obtain the targeted compounds of this new series, is based on a synthetic route already reported in literature and used for similar compounds *via* Kneovenagel condensation reaction [13]. Following the same procedure, compounds **6a-f** has been synthesized by reacting 4,4',6,6'-tetramethyl-2,2'-bipyrimidine with the corresponding aldehyde **5a-f** in NaOH 5M in presence of Aliquat 336. The compounds **6a-f** were obtained in reasonable yields (~30-40 %) and further fully characterized by NMR, UV-vis, mass spectroscopy and elemental analysis, confirming the expected molecular structure and the symmetrical substitution pattern on the bipyrimidine core.

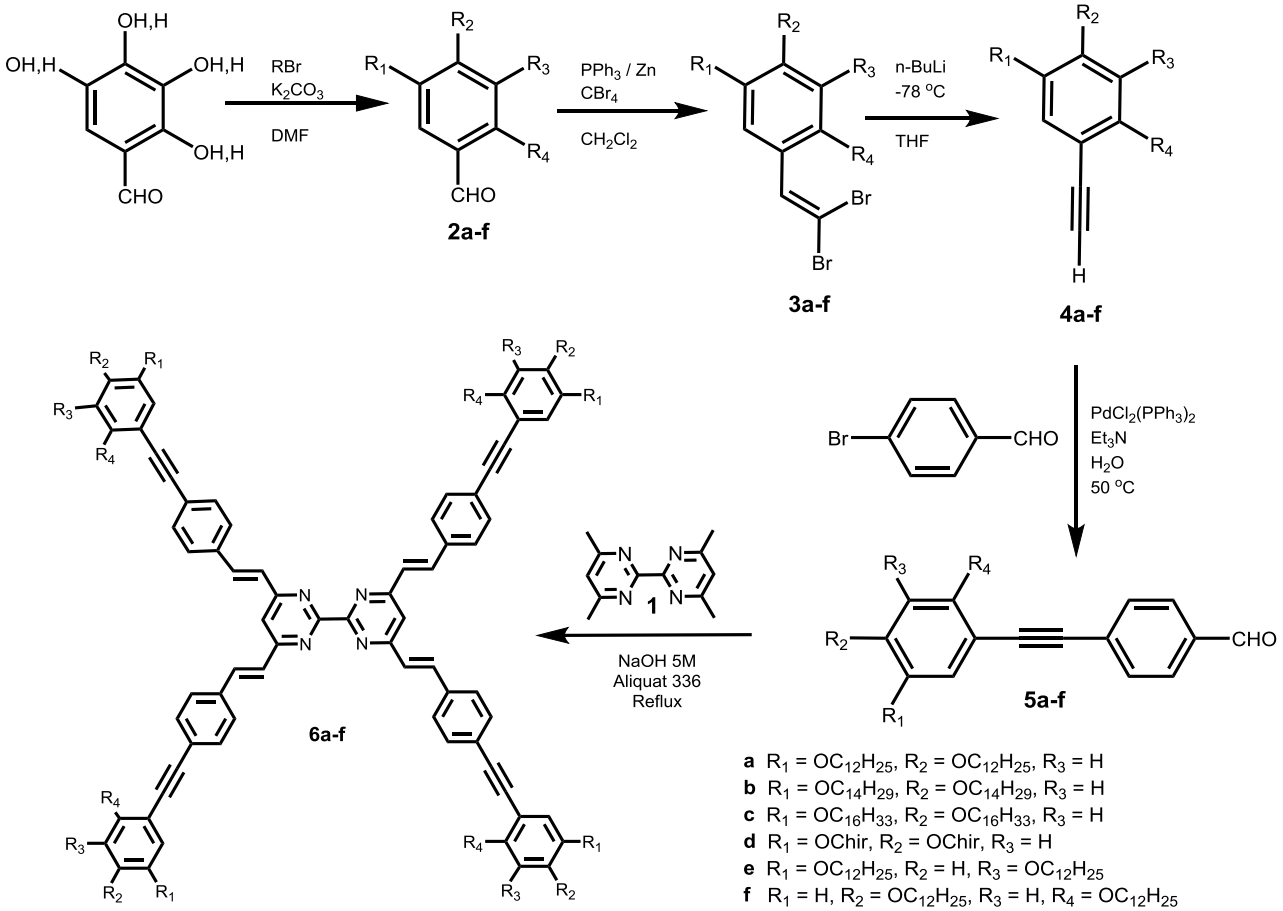

Scheme 1. Synthesis scheme of targeted compounds **6a-f**.

Thermal Behavior and Self-Organization Properties.

The thermal properties of the various BPM compounds were studied by combining polarized-light optical microscopy (POM) observations and differential scanning calorimetry (DSC) measurements, whereas the molecular organizations in the various phases were analyzed by small-angle X-ray scattering (SAXS) experiments. The thermal behaviors are summarized in Table 1.

The DSC trace of **6a** compounds shows no transition on the cooling curves whereas, on heating, an exothermic peak directly followed by an endothermic peak is observed (See ESI). Such thermal behavior is typical of compounds whose molecular organization is strongly constrained. The thermal energy imported during heating allows the compound to find a better way to reorganize itself, which is what causes the exothermic transformation. SAXS patterns confirm that above 100 °C, the compound is in an isotropic state and that on cooling from high temperatures, the compound slowly reorganized into a poorly defined mesophase (Figure 1a). The SAXS patterns display in the small angle region two sharp diffraction peaks which can be tentatively indexed, based on the indexation of the other compounds (see below), as the (10) and (20) reflections from a 2D hexagonal lattice (Figure 2a). The broad halo (h_{ch}) observed around 20 ° in 2θ confirms that the compound is in a liquid state. The combination of DSC and SAXS measurements thus reveals that this compound slowly reorganized into a columnar mesophase with hexagonal symmetry on cooling below 90 °C and that this mesophase persists down to -25 °C. Upon heating this compound remains in this mesomorphic sate and the exothermic peak observed on the DSC heating trace is due some internal reorganization inside the LC phase, with no noticeable effect on the SAXS patterns.

Table 1. Thermal Behaviors of the **6a-f** derivatives.

	Transition temperatures °C (ΔH in J.g^{-1})	**d_{meas}/Å**	**hk**	**Mesophase parameters measured at T**
6a	Col_h 91.8 (9.6) Iso Iso 90* Col_h	44.53 23.54 4.34	10 20 h_{ch}	Col_h T = 30 °C a = 51.42 Å
6b	Cr 9.3(25.5) Col_h 172.6(1.0) Iso Iso 169.1(-1.1) Col_h 4.8(-21.9) Cr	44.53 25.99 22.48 16.93 4.46 3.91 3.76 3.47	10 11 20 21 h_{ch} h_{stack} h'_{stack} h''_{stack}	Col_h T = 90 °C a = 51.42 Å
6c	Cr1 36.3(29.3) Cr2 78.8(12.8) Cr3 91.2(0.6) Iso Iso 67.0 Cr3 40.5 Cr2 29.3 Cr1**			-
6f	LCx -2.2(-24.05) Cr 31.5(10.3) LCx 70.7(1.9) Iso Iso 48.8(7.1) LCx			LCx
6e	Amorphous			-
6d	Col_h 137.5 Iso*** Iso 132 Col_h	37.44 21.54 18.78 14.09 4.63	10 11 20 21 h_{ch}	Col_h T = 40 °C a = 43.23 Å

[a] Heating and cooling processes were carried out with a "Perkin-Elmer DSC-4000" device at a rate of 10.0°C/minute. Enthalpy values are given in brackets. *Value extracted from SAXS measurements; **DSC integrations could not have been performed correctly; *** values extracted from the POM observations; Cr: crystal; LCx: unidentified liquid crystal; Colh: hexagonal columnar phase; Iso: isotropic phase.

The **6b** compound is in a liquid crystalline state over a large temperature range between 7 and 171 °C (Table 1). The pseudo-fan-shaped fluid textures observed in the mesomorphic range are characteristic of a columnar mesophase (Figure 1b). SAXS patterns recorded between room temperature and the isotropization temperature are all characteristic of a columnar mesophase of hexagonal symmetry (Figure 2b). The sharp peaks in the small angle region can unambiguously be indexed in a 2D hexagonal lattice and a broad halo (h_{ch}) in the wide-angle region confirms that the long carbon chains are in a molten state. A series of sharp diffraction peaks (h_{stack}) is also observed in the wide angle and indicates that the aromatic parts are well organized inside the columnar core. Previous x-rays diffraction analyses on single crystal, DFT calculations and IR spectroscopy have demonstrated that bipyrimidine molecules can be non-planar in solid state and can adopt a pseudo-tetrahedral configuration with a dihedral angle between the two pyrimidine fragments around 70°. Previous molecular packing investigations on bipyrimidine cores presenting alkoxystyryl donor groups carrying aliphatic chains in the 3,4 position have also revealed that these compounds are interdigitated alternatively along their long axis and their short axis to form columns [13]. The same columnar molecular packing can be envisioned for this new series of compounds.

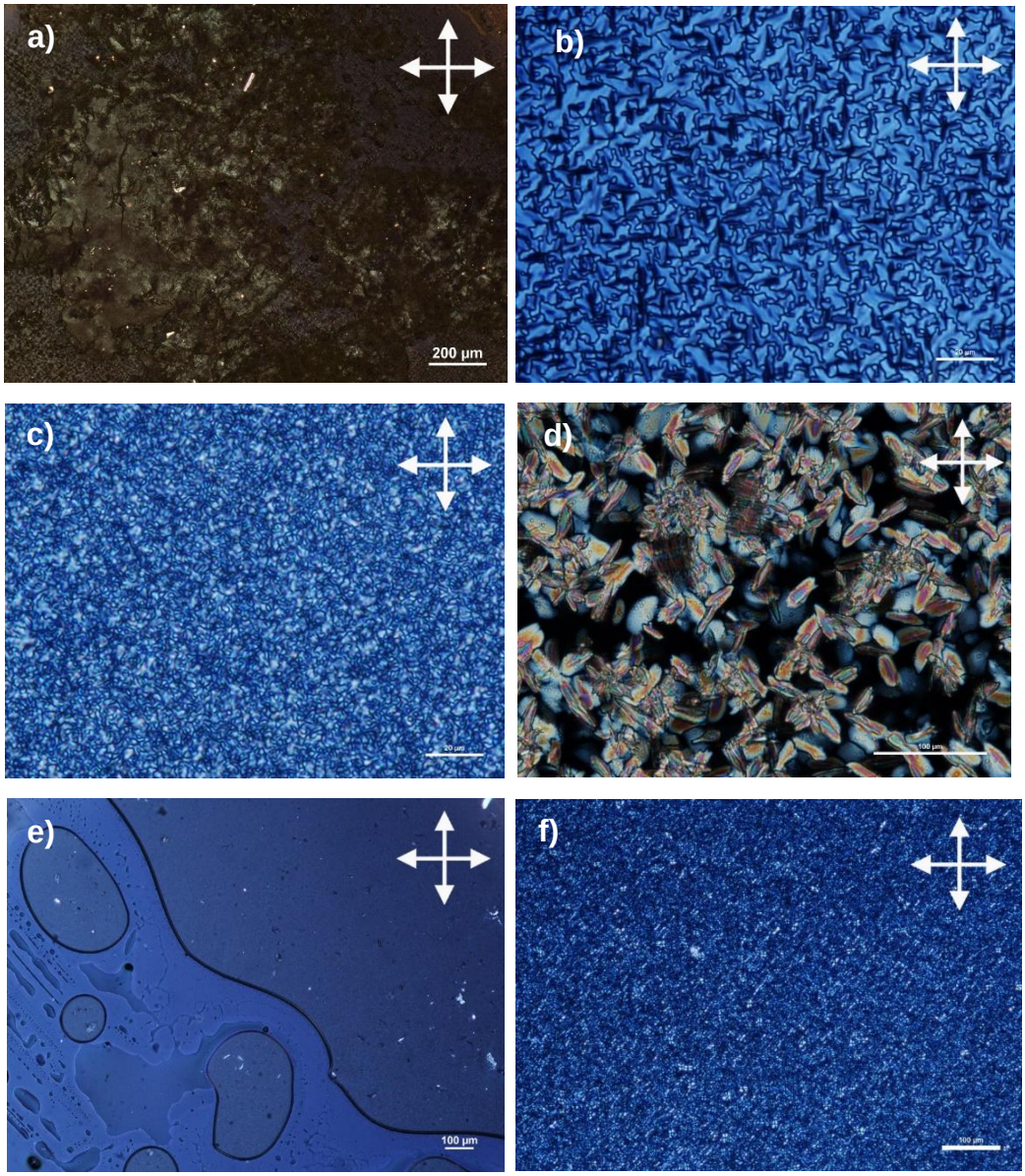

Figure 1. POM images by optical microscopy between crossed-polarizers (crossed-polarizers symbolized by the white cross in the corner of the picture) (a) Compound **6a** at 43 °C during cooling from the isotropic phase (b) Pseudo-fan shaped texture observed with **6b**compound at 142 °C on cooling from the isotropic state (c) Compound **6c** recorded at 20 °C on cooling from the isotropic phase (d) Compound **6d** recorded at 119 °C on cooling from the isotropic phase (e) The pristine compound **6e** at 20 °C (f) Compound **6f** recorded at 52 °C upon cooling from the isotropic phase.

POM observations for compound **6c** shows that above 100 °C, the compound is in an isotropic state. Upon cooling from the isotropic state around 60 °C, an uncharacteristic and hardly deformable texture start to develop (Figure 1c). SAXS measurements confirm the crystallization of the compound below 60 °C. Indeed, the SAXS patterns display several sharp peaks over the whole small angle region together with a structured broad halo around 20° in 2θ (Figure 2). Upon heating, the SAXS patterns show that the compound remains crystalline up to the isotropization temperature found around 100 °C. Thus, all the broad thermal transitions detected on the DSC below 60 °C on cooling and 100 °C on heating are attributed to crystal to crystal transformations. This compound is deprived of mesomorphic properties.

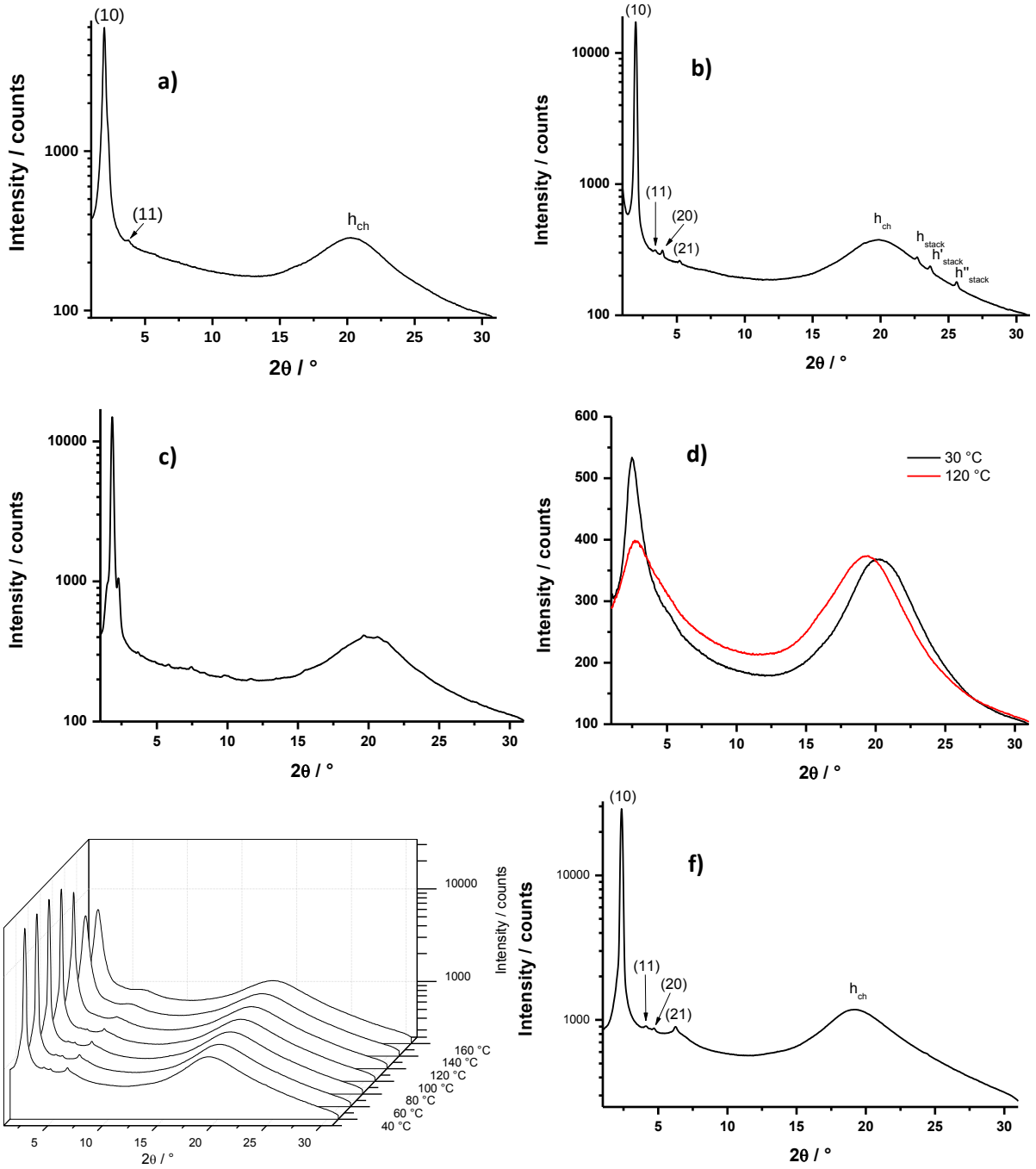

Figure 2. SAXS patterns of (a) **6a** compound recorded at 30 °C after heating at 180 °C (b) of **6b** compound recorded at 80 °C upon heating (c) Compound **6c** recorded at 80 °C upon heating (d) Compound **6e** recorded at 120 and 30 °C upon cooling. (e) Temperature-dependent SAXS patterns recorded on compound **6d** on cooling from the isotropic state (1st cooling) (f) SAXS pattern of compound **6d** recorded at 40 °C after cooling from the isotropic phase (1st cooling).

The compound **6e** appears as a soft and completely black material under crossed polarizers (Figure 1e), confirming that this compound is amorphous and is completely devoid of mesomorphic properties. As already observed on bipyrimidine compounds with shorter arms [13], the substitution with long carbon chains at the 3,5 position prevents any proper molecular organization.

The DSC cooling curves of **6f** compound display a single exothermic transition centered at 49 °C (Table 1, Figure ESI). At 120 °C, the compound is in an isotropic state, as confirmed by POM

observations, and the recorded SAXS pattern displays only one single broad peak in the small angle region and a broad halo in the wide-angle region, corresponding the long and short dimensions of the molecule. Upon cooling, a clear sharpening of the small angle diffraction peak is observed between 60 and 40 °C and point to the formation a more organized phase. POM observations performed upon cooling from the isotropic phase show that a fluid texture readily developed around 50 °C (Figure 1f) and confirmed the formation of a liquid crystalline phase. However, the lack of higher order diffraction peaks on the SAXS patterns in the small angle region and the formation of an uncharacteristic texture prevent any clear phase symmetry assignment (Figure 2f). The heating curves appear much more complicated with, at least, one clear exothermic and two endothermic peaks. The broad exothermic peak centered at -2 °C is likely attributed to a crystallization of the compound and the broad endothermic peak centered at 31.5 °C to the melting of the crystalline phase into a mesomorphic state. The presence of the exothermic peak upon heating reveals that the molecular reorganization is strongly hindered during the cooling process. Storing such a compound for a long period of time at low temperature will certainly result in slow crystallization of the compound. The SAXS patterns recorded upon heating show that the compound is in liquid crystalline state between 30 and 60 °C and, that at higher temperatures, the compound melt into an isotropic phase. These results confirm that this compound can indeed exhibit mesomorphic properties but they are highly dependent on the thermal history of the compound.

At room temperature, **6d** compound appears as a birefringent fluid gel between crossed polarizers, good indication of its liquid crystalline nature. The compound became fully isotropic at 140 °C. Upon cooling, a texture started to develop below 132 °C. The texture combining mosaics with linear and pseudo-fan shaped birefringent defects together with homeotropic regions is typical of hexagonal columnar (Col_h) (Figure 1d). The fluidity and the texture are preserved down to room temperature. Upon further heating, a clear transition into the isotropic phase was detected at 137.5 °C. This Col_h/Iso transition is low-energy transition and no marked peak associated to a phase transition could have been properly identified on the DSC traces between -25 and 150 °C (Table 1, Figure ESI). The temperature-dependent SAXS investigations unambiguously confirmed the transition temperature and the formation of a columnar mesophase of hexagonal symmetry. The isotropic to col_h transition is characterized on the SAXS patterns by the sharpening and the strong increase in intensity of the first order diffraction peak between 140 and 120 °C on cooling (Figure 2d). The SAXS patterns recorded below 120 °C are all characteristic of a columnar liquid crystalline phase of hexagonal symmetry. In the small angle region, the first reflections and its higher orders can be unambiguously indexed into a 2D hexagonal lattice and the broad halo centered on 4.6 Å confirms that the fluid nature of the phase (Figure 2d). On heating, the isotropization is also observed between 120 and 140 °C and is characterized by a broadening of the 1^{st} order refection and a strong decrease of its intensity, together with a disappearance of the higher order reflections. Based on the POM, DSC and SAXS investigations, it can be concluded that this compound forms a columnar mesophase of hexagonal symmetry between -25 and 130 °C.

Linear and Nonlinear Optical Properties in Solution.

Figure 3 displays the one- and two-photon absorption spectra of the chromophores along with their respective fluorescence bands in THF. Table 2 gathers the corresponding spectroscopic data in the same solvent. For all the derivatives, the low energy region of the one-photon absorption (1PA) spectrum is dominated by a single absorption band in the 330-450 nm range. The intensity and the

maximum absorption wavelength of the 1PA bands are clearly sensitive to the positioning of the external alkoxy substituents.

Note that all the *para*-substituted dyes exhibit very high ε_{MAX} (~ 120 000 M^{-1} cm^{-1}) suggesting the occurrence of strongly allowed electronic transitions within the 1PA band. As previously observed for similar bipyrimidine-based octupoles [13,19] this absorption band is known to encompass several $\pi\pi^*$–type transitions implying an intramolecular charge transfer (ICT) character with a long-range electronic delocalization from the alkoxy donor groups to the bipyrimidine electron deficient subunit.

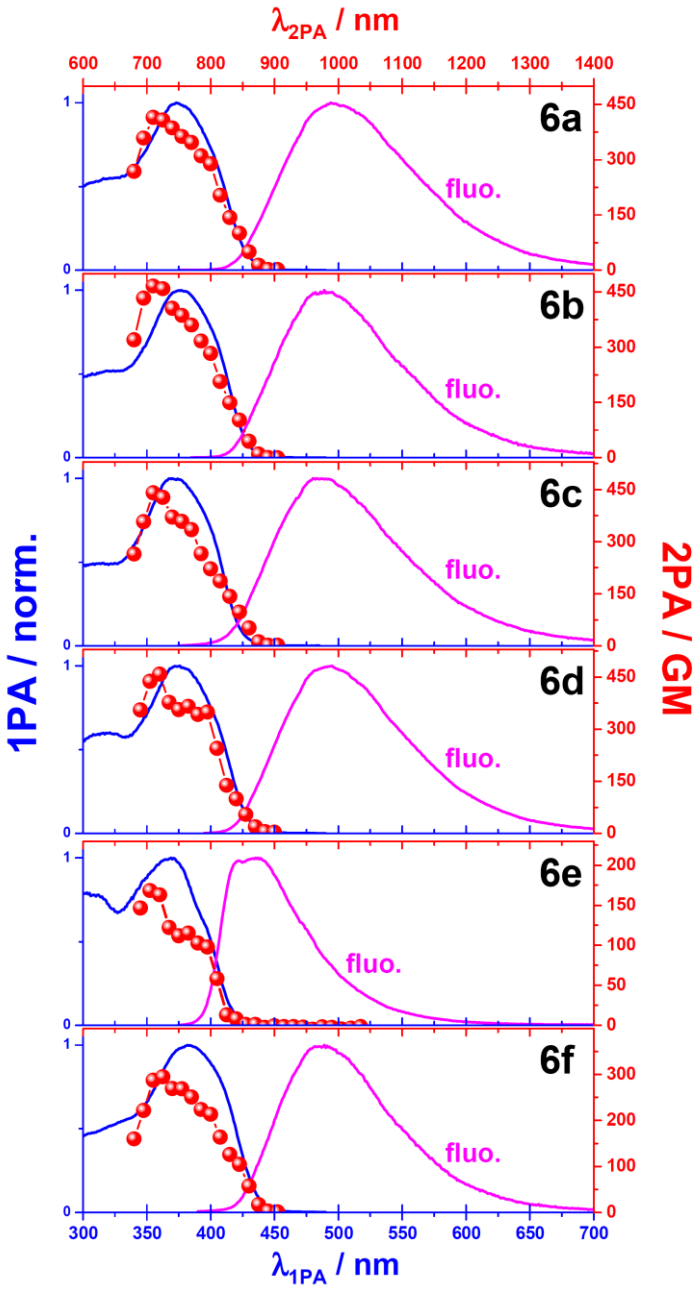

Figure 3. 1PA (blue lines), 2PA (red circles) and fluorescence spectra of chromophores in **THF**.

Here also, the efficiency of the ICT process can be amplified by a *meta*-to-*para* positioning of the alkoxy substituents. For instance, ongoing from the 3,5-disubstitued dye (**6e**) to the 3,4-ones, the 1PA band undergoes a 1.3-fold increase in intensity associated with a red shift of about 860 cm^{-1}. This

bathochromic effect is more significant when considering the fluorescence band, which shifts to the low energy region by about 2500 cm^{-1} ongoing from the *meta* to the *para* dyes.

Table 2. One- and Two-Photon Spectroscopic data of compounds in THF.

	ε_{abs} 10^3 M^{-1} cm^{-1}	λ_{1P} nm	λ_{fluo} nm	E_{00} [(1)] eV	Φ_{fluo}	τ_{fluo} [(2)] ns	k_r [(3)] 10^9 s^{-1}	k_{nr} [(3)] 10^9 s^{-1}	$\frac{k_{nr}}{k_r}$	λ_{2P} nm	δ_{2P} [(4)] GM
6a	118.7	377	496	2.90	0.84	1.96	0.43	0.08	0.19	710	**415**
6b	129.6	380	488	2.91	0.89	2.01	0.44	0.05	0.12	710	**466**
6c	121.1	378	487	2.92	0.81	1.97	0.41	0.10	0.23	710	**441**
6d	120.0	378	492	2.90	0.78	2.02	0.39	0.11	0.28	720	**458**
6e	95.2	368	437	3.11	0.33	0.87	0.38	0.77	2.03	705	**168**
6f	**101.1**	**388**	**487**	**2.87**	**0.86**	**2.02**	**0.43**	**0.07**	**0.16**	**725**	**295**

[(1)] $E_{00} \approx ½\ hc(\nu_{abs} + \nu_{fluo})$ [(2)] Average fluorescence lifetime from a bi-exponential fit [(3)] $k_r = \Phi_{fluo}/\tau_{fluo}$ and $k_{nr} = (1- \Phi_{fluo})/\tau_{fluo}$
[(4)] The uncertainty in δ is ± 15%.

As shown in Table 2, all the *para* chromophores are extremely emissive with fluorescent quantum yields ($\Phi_{fluo.}$) higher than 0.75. It should be noted that the corresponding radiative rate constants (k_r) are 5-fold larger than their respective non-radiative ones (k_{nr}) confirming that the fluorescence process constitutes the major S_1-state deactivation route which implies a highly emissive ^{1}ICT state [20]. Interestingly, the energy of this low-lying excited state clearly rises on going from *para* to *meta* derivatives (ΔE ~ 0.2 eV). This effect opens up additional non-radiative channels which competes with fluorescence and drastically increases the k_{nr}-to-k_r ratio whose value is amplified by a factor 10 (Table 2). In the same manner, the *meta*-to-*para* positioning effect strongly impacts the two-photon absorption (2PA) performances of the octupolar series. Whereas the maximum 2PA cross section (δ_{MAX}) of **6e** hardly reaches a value of ca. ~170 GM, the corresponding δ_{MAX} for the 3, 4-disubstitued derivatives display a significant value of about ~ 450 GM. It should be noted that this latter average value is 100 GM higher than that previously measured for similar octupoles which integrates shorter stilbenyl branches [20]. This structural difference obviously confirms that increasing the effective conjugation length within each D-π-A branch of the octupoles results in a substantial enhancement of their 2PA performance. As shown in Figure 3, all the dyes display similar 2PA bands, which do not coincide, with their respective 1PA ones. This spectral effect is usually observed for octupolar architectures with a D_{2d} centrosymmetry [13,19,20] and leads to a $S_0 \rightarrow S_1$ transition, which is theoretically two-photon forbidden [21]. As a consequence, the 2PA band which is blue shifted as compared to the 1PA one should be attributed to a high-lying $S_0 \rightarrow S_n$ transition.

Hyper-Rayleigh Scattering (HRS) was employed to try to confirm the octupolar second-order nonlinear optical properties of these extended bipyrimidine based derivatives. From the identical D2 topology for these chromophores when compared to similar bipyrimidine derivatives with shorter alkoxystyryl groups attached to this pseudotetrahedral core, it was expected that the first hyperpolarisability (second-order nonlinear molecular hyperpolarisability) to be identical. Such an observation would be in line with earlier observations with both achiral and chiral alkoxy groups [13]; independent of the substitution pattern on the bipyrimidine (3,4-di; 3,5-di; 3,4,5-tri) and also independent of alkoxy chain length (between C12 and C16) [19].
HRS experiments were performed in chloroform at 1300 nm. This wavelength was selected for comparison with the earlier measurements, and with the aim to avoid multiphoton fluorescence (MPF) contribution to the HRS signal. Such MPF contributions have been observed and dealt with in the earlier

reports, either with active MPF suppression and the determination of a fluorescence lifetime in the frequency domain [13] or with discrimination between a narrow HRS peak on a broad MPF background in the spectral domain [19].

However, for the substitution pattern here with longer alkoxystyryl groups on the octupolar bipyrimidine core, the fluorescence, and also the MPF, has red-shifted, from around 430 nm for the shorter alkoxy groups [13,19] to around 490 nm. Together with the much stronger fluorescence quantum yield observed here, 0.74 for the styrylalkynyl derivatives versus 0.12 for the styryl derivatives [13,19], the MPF contribution overwhelmed the HRS and no HRS peak could be detected on the strong and broad MPF background. The experimental observations are still in agreement with what can be expected from the earlier reported first hyperpolarisability values (static value derived from the three-level model for octupoles $\beta_{HRS,0}$ between 38 +/- 8 and 66 +/-15) [13,19], which all were clearly governed by the presence of the octupolar bipyrimidine core (HRS depolarization ratio around 2) [19] that is also present here.

Shifting the tunable fundamental laser wavelength from 1300 nm to shorter wavelengths (tuning range is 800 – 1300 nm) would have led to stronger two-photon absorption (see TPA spectra and discussion, Fig. 3 and Table 2). Note finally that from the apolar nature of the tetrasubstituted bipyrimidine, only HRS is capable of experimentally providing a value for the first hyperpolarisability. Electric-field-induced Second-Harmonic Generation (EFISGH) is not appropriate as the octupolar chromophore with D2 topology does not possess a dipole moment to interact with the static electric field.

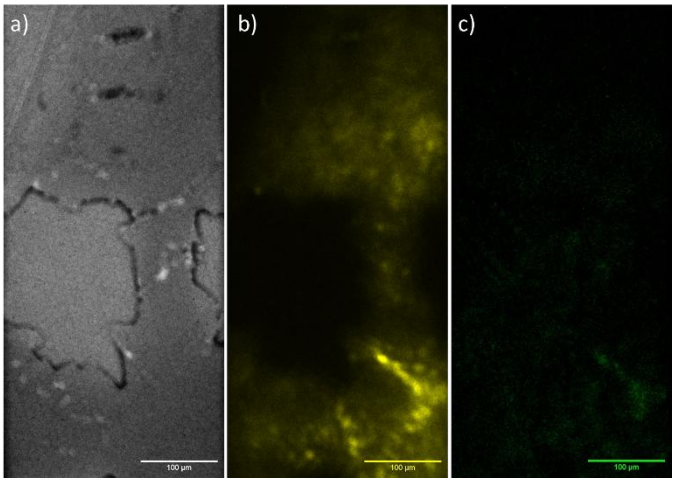

Figure 4. Recorded images of compound **6d** after recrystallization. (a) Brightfield image of compound **6d** illuminated by a LED source. Captured MPF (b) and SHG (c) image of compound **6d**. The MPF and SHG images were obtained at a laser beam power of 824 mW.

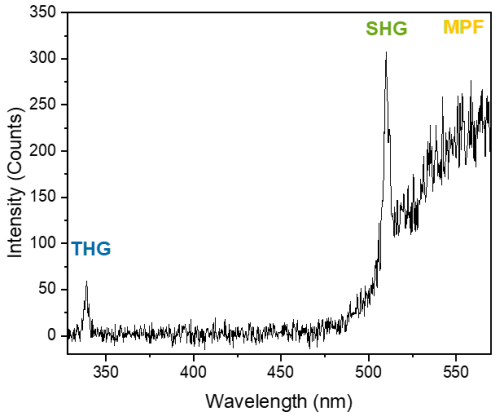

Figure 5. Spectral measurement obtained for compound **6d**. The spectrum shows a THG peak at 343 nm and a SHG peak at 515nm. The spectrum was obtained at a beam power of 824 mW.

Nonlinear optical microscopy. We used widefield second harmonic generation (SHG) microscopy to interrogate the second-order nonlinear optical properties in the solid state. Measurements were conducted at room temperature with a setup detailed in prior research and operating at 1030 nm [19]. Since SHG only occurs efficiently for materials that lack inversion symmetry, it requires that the bipyrimidine chromophores are organized in a noncentrosymmetric manner. Prior studies [22] on structurally related bipyrimidine derivatives have demonstrated that chiral side chains can trigger supramolecular chirality, resulting in a strong SHG response. However, despite its chiral side chains, compound **6d** initially did not show any measurable SHG signal, due to its tendency to form amorphous

films. Only after slow recrystallization small crystalline domains emerged. These domains show SHG activity, as shown in Figure 4. Spectral measurements further demonstrated the emergence of an SHG peak at 515 nm (Figure 5). The spectrum further shows a broad multiphoton fluorescent background and a peak originating from third harmonic generation (THG) at 343 nm. In line with previous observations on related bipyrimidine derivatives, these results show that the solid state second-order nonlinear optical response crucially relies on the efficient transfer of molecular to supramolecular chirality.

Conclusion

In conclusion, a new series of octupolar four-branched compounds incorporating a bipyrimidine chelating group as an electron-deficient core and four divergent lipophilic styryl-alkynyl fragments bearing alkoxy-substituted groups in the 3,4 / 3,5 / 2,4 positions have been synthesized. The introduction of long carbon chains at the 3,4 position, for chain lengths below 14 carbons, allows the emergence of columnar mesophases with hexagonal symmetry over wide temperature ranges. Introduction of carbon chains in the 2,4 positions, strongly hindered the molecular organization and leads to the formation of poorly defined mesophase. The carbon chains in position 2 are probably intercalated between the aromatics along the columnar stacks. And finally, as already observed, introduction of long carbons chains in the 3,5 positions completely prevents the interdigitation of the byprimidine cores and also any molecular organization. All the *para* chromophores are extremely emissive around 490 nm with quantum yields ($\Phi_{fluo.}$) around 80 % and displaying interesting second and cubic NLO activities at the molecular level in solution in line with previous bipyrimidine derivatives [13,19]. This structural difference obviously confirms that increasing the effective conjugation length within each D-π–A branch of the octupoles results in a substantial enhancement of their 2PA performance. Finally, the crucial efficient transfer of chirality from molecule to supramolecular material lead to non-centrosymmetric organization resulting in a strong Second Harmonic Generation at the solid state.

Experimental Section

NMR spectra (^{1}H, ^{13}C) were recorded at room temperature on BRUKER Avance III 500 spectrometer, in $CDCl_3$ solution, with tetramethylsilane as external standard.

Microanalysis was performed using a Thermo Fischer Scientific FlashEA 1112 Series elemental analyzer.

Mass spectra were obtained on a Bruker Micro-TOF-Q II instrument and a Q-TOF-LC-MS/MS instrument.

Steady-state absorption and fluorescence spectra. The absorption measurements were carried out with a Perkin Elmer Lambda 2 spectrometer. Steady-state fluorescence spectra were collected from a FluoroMax-4 spectrofluorometer. Emission spectra are spectrally corrected, and fluorescence quantum yields include the correction due to solvent refractive index and were determined relative to quinine bisulfate in 0.05 molar sulfuric acid (Φ_{ref} = 0.52) [23].

Differential scanning calorimetry (**DSC**) was carried out by using NETZSCH DSC 200 F3 instrument equipped with an intracooler. DSC traces were measured at 10 °C/min down to -25 °C.

Optical microscopy investigations were performed on a Nikon H600L polarising microscope equipped with a Linkam "liquid crystal pro system" hotstage. The microscope is also equipped with a UV irradiation source (Hg Lamp, λ = 350-400 nm) and an ocean optic USB 2000+ UV-Vis-NIR spectrophotometer based on CCD detection technology. This set-up allows the recording of luminescence spectra on solids, liquids, liquid crystalline materials and gels from -196°C up to 420°C between 350 and 1100 nm.

Time-correlated single photon counting. The fluorescence lifetimes were measured using a Nano LED emitting at 372 nm as an excitation source with a nano led controller module, Fluorohub from IBH, operating at 1MHz. The detection was

based on an R928P type photomultiplier from Hamamatsu with high sensitivity photon-counting mode. The decays were fitted with the iterative reconvolution method on the basis of the Marquardt/Levenberg algorithm [24]. Such a reconvolution technique allows an overall-time resolution down to 0.15 ns. The quality of the exponential fits was checked using the reduced χ^2 ($\leq$ 1.2).

Two-photon excited fluorescence. The two-photon absorption measurements were performed with femtosecond mode-locked laser pulse using a Ti: Sapphire laser (Coherent, Chameleon Ultra II: pulse duration: ~140 fs; repetition rate: 80 MHz; wavelength range: 680-1080 nm). A relative two-photon excited fluorescence (2PEF) method [25] was employed to measure the two-photon absorption cross-sections, δ. A 10^{-4} M solution of fluorescein [24] in water at pH = 11 was used as the reference (r). The value of δ for a sample (s) is given by:

$$\delta_S = \frac{S_S \Phi_r \eta_r c_r}{S_r \Phi_S \eta_S c_S} . \delta_r$$

where S is the detected two-photon excited fluorescence integral area, c the concentration of the chromophores, and Φ is the fluorescence quantum yield of the chromophores. η is the collection efficiency of the experimental set-up and accounts for the wavelength dependence of the detectors and optics as well as the difference in refractive indices between the solvents in which the reference and sample compounds are dissolved. The measurements were conducted in a regime where the fluorescence signal showed a quadratic dependence on the intensity of the excitation beam, as expected for two-photon induced emission. For the calibration of the two-photon absorption spectra, the two-photon excited fluorescence signal of each compound was recorded at the same excitation wavelength (λ_{exc}: 782 nm) as that used for fluorescein. The laser intensity was in the range of 0.2-2 x 10^9 W/cm^2. The experimental error on the reported cross section is 15 %.

Hyper-Rayleigh scattering: A custom designed optical setup was used to determine the first hyperpolarizabilities of the compounds. The laser (Insight DS+, Spectra-Physics) allows for a tunable output between 680 and 1300 nm. The former delivers femtosecond (~120 fs) pulses at an 80 MHz repetition rate. The output beam ($1/e^2$ < 1.2 mm) has a gaussian profile (M^2 < 1.1) is horizontally polarized (the plane of the optical table). A combination of an achromatic half-wave plate and Glan-Laser polarizer allows to control the output power in accordance to Malus's law. The polarizer is placed in such a way that the extraordinary ray is vertically polarized. The average power which is sent into the sample typically ranges from 500 to 1000 mW. The beam is routed to the input lens (aspheric, f = 8.00 mm) by a series of mirrors. A long pass filter with a cut-off at 690 nm is used to prevent any higher harmonic generation from the laser or the optics from entering the sample. The quartz cuvette (10x4 mm) is placed in a custom translation mount which allows to define the path length of the focal point relative to the side walls. Light is collected at 90° by an achromatic, aspheric condenser lens (f = 30 mm). The collimated beam passes a series of three large broadband dielectric elliptical mirrors to rotate the image 90°. The latter ensures maximal resolution of the spectrograph (vertically oriented slit). The collimated beam is focused on the spectrograph (IS/SM 500, Bruker) with a plano-convex lens, matching the focal length of the spectrograph (f = 200mm, f/8). A blocking edge filter (FF01-720/SP-25, Semrock) ensures high optical density in the laser excitation range. One of two gratings (50 grooves/mm, 600nm blaze or 150 grooves/mm, 500nm blaze) were used, depending on the desired resolution, diffraction range and spectral profile of multiphoton emission spectra. An EMCCD camera (Ixon Ultra 897, Andor Solis) was used to image the spectra.

Nonlinear optical microscopy. Widefield illumination of the sample was performed under normal incidence with femtosecond pulsed infrared (IR) laser light at 1030 nm (Pharos, Light Conversion). The incident laser light intensity and polarization are varied by 2 sets of computer-controlled half-wave plate and polarizer (in P-direction) combinations, located immediately after the laser system. The resulting S-polarization of the incident IR laser light was obtained by a final half-wave plate. The sample is irradiated by a long focal length lens (f=35 mm,Thorlabs, LA1027-A-ML) which is focused above the sample, so that the incident fundamental light can be considered to a good approximation as a collimated beam and electric field components along the propagation direction (Z) can be neglected. Behind the sample, a 20x objective (Nikon, CFI Plan Fluor 20X CH) collects the light. In the infinity path an IR filter rejects the laser light and a filter wheel selects the transmitted wavelength for SHG (Bandpass, 515 nm, Edmund Optics #65-153), MPF (Longpass, Cut-off wavelength 525 nm, Edmund Optics #84-744) or Bright field (no filter). A 20 cm tube lens (Mitutoyo) then images the light onto the slit of an imaging spectrometer (Andor, Kymera 328i), coupled to an I-CCD camera (Andor, iStar DH334-18U). By switching between a mirror and a grating (150 l/mm groove density; blaze=500 NM), the spectrometer can be used for imaging and spectroscopy respectively. The latter option requires closing the slit of the spectrometer to ensure adequate spectral resolution. For the bright field imaging, an LED source mounted above the sample was used. This LED source could be polarization selected by

a broadband polarizing sheet, positioned perpendicular to a rotatable broadband polarizer in the detection path. In this manner, polarized optical microscopy images could be recorded.
The samples were heated up to 190°C and subsequently cooled to room temperature using a Linkam LTS350 stage coupled to Linkam TP94. The achieved heating and cooling rates between the two temperatures was 10°C/min. The heating and cooling cycle was repeated three times to recrystallize the samples before measurement.

X-ray scattering experiments (SAXS) were performed using a XENOCS microsource (50W) with monochromatic Cu Kα radiation (λ = 1.541 Å) and point collimation. The patterns were collected with a Mar345 Image-Plate detector (Marresearch, Norderstedt, Germany). The exposure time at each temperature was 3600 s and the heating or cooling speed between two temperatures was 10 °C/min. The samples were held in Lindeman glass capillaries (1.5 mm diameter). The capillaries were placed inside a Linkam HFX350-Capillary X-Ray stage which allow measurements from -196 °C up to 350 °C with an accuracy of 0.1 °C.

All reagents for synthesis were commercially obtained from Aldrich. The solvents employed for the analysis were spectroscopic grade. All the intermediates **2**, **3**, **4** and **5** are already described and were synthesized according to the literature (See refs 16, 17, 18) and characterized par ^{1}H and ^{13}C NMR.

General Procedure for Compounds 2a-f: Commercially available 3,4-dihydroxybenzaldeyde (50 mmol) and K_2CO_3 (125 mmol) were stirred in dry DMF (50 mL) at 75 ^{o}C under argon atmosphere for 1h. Then related carbon numbered alkyl bromide (125 mmol) compounds are slowly added to reaction mixture and are stirred at 150 ^{o}C for 24h. The reaction was monitored by TLC (H/EA 5:1). The reaction mixture was filtered over silica gel and the solvent was removed under reduced pressure. The crude product was purified by column chromatography on silica gel eluting with hexane/ethyl acetate mixtures (H: EA / 5: 1).

3,4-bis(dodecyloxy)benzaldehyde (2a): ($C_{31}H_{54}O_3$; 474,77 g/mol)
Yield: 19 g (80%), white powder. ^{1}H NMR (500 MHz, $CDCl_3$): δ (ppm) = 9.83 (s, 1H, CHO), 7.41 (dd, J ≈ 8.2 and J ≈ 2.0 Hz, 1H, Ar-H), 7.39 (d, J ≈ 1.5 Hz, 1H, Ar-H), 6.95 (dd, J ≈ 8.1 and J ≈ 1.8 Hz, 1H, Ar-H), 4.13 – 3.99 (m, 4H, OCH_2), 1.91 – 1.79 (m, 4H, CH_2), 1.61 – 1.16 (m, 36H, CH_2), 0.89 (t, J ≈ 7.0 Hz, 6H, CH_3). ^{13}C NMR (125 MHz, $CDCl_3$): δ (ppm) = 191.18 (CHO), 154.83, 149.58, 111.10 (Ar-C), 130.01, 126.75, 111.90 (Ar-CH), 69.29, 69.27 (OCH_2), 32.07, 29.84, 29.80, 29.76, 29.75, 29.53, 29.51, 29.21, 29.12, 26.13, 26.09, 22.84 (CH_2), 14.26 (CH_3).

3,4-bis(tetradecyloxy)benzaldehyde (2b): ($C_{35}H_{62}O_3$; 530,88 g/mol)
Yield: 20.7 g (78%), white powder. ^{1}H NMR (500 MHz, $CDCl_3$): δ (ppm) = 9.83 (s, 1H, CHO), 7.41 (dd, J ≈ 8.1 and J ≈ 1.8 Hz, 1H, Ar-H), 7.39 (d, J ≈ 1.8 Hz, 1H, Ar-H), 6.95 (d, J ≈ 8.1 Hz, 1H, Ar-H), 4.11 – 4.00 (m, 4H, OCH_2), 1.92 – 1.79 (m, 4H, CH_2), 1.60 – 1.20 (m, 44H, CH_2), 0.88 (t, J ≈ 6.9 Hz, 6H, CH_3). ^{13}C NMR (125 MHz, $CDCl_3$): δ (ppm) = 191.17 (CHO), 154.94, 149.59, 111.09 (Ar-C), 130.01, 126.75, 111.89 (Ar-CH), 69.29, 69.27 (OCH_2), 32.08, 29.86, 29.82, 29.77, 29.75, 29.53, 29.52, 29.22, 29.13, 26.14, 26.10, 22.84 (CH_2), 14.27 (CH_3).

3,4-bis(hexadecyloxy)benzaldehyde (2c): ($C_{39}H_{70}O_3$; 586,99 g/mol)
Yield: 22 g (75%), white powder. ^{1}H NMR (500 MHz, $CDCl_3$): δ (ppm) = 9.83 (s, 1H, CHO), 7.41 (dd, J ≈ 8.1 and J ≈ 1.7 Hz, 1H, Ar-H), 7.39 (d, J ≈ 1.6 Hz, 1H, Ar-H), 6.95 (d, J ≈ 8.1 Hz, 1H, Ar-H), 4.15 – 3.96 (m, 4H, OCH_2), 1.91 – 1.79 (m, 4H, CH_2), 1.59 – 1.22 (m, 52H, CH_2), 0.88 (t, J ≈ 6.9 Hz, 6H, CH_3). ^{13}C NMR (125 MHz, $CDCl_3$): δ (ppm) = 191.17 (CHO), 154.83, 149.59, 111.09 (Ar-C), 130.01, 126.75, 111.89 (Ar-CH), 69.29, 69.27 (OCH_2), 32.08, 29.86, 29.82, 29.77, 29.76, 29.54, 29.52, 29.22, 29.13, 26.14, 26.10, 22.84 (CH_2), 14.27 (CH_3).

3,4-bis(((*S*)-3,7-dimethyloctyl)oxy)benzaldehyde (2d): ($C_{27}H_{46}O_3$; 418,66 g/mol)
Yield: 16.5 g (79%), light yellow liquid. ^{1}H NMR (500 MHz, $CDCl_3$): δ (ppm) = 9.83 (s, 1H, CHO), 7.42 (dd, J ≈ 8.1 and J ≈ 1.9 Hz, 1H, Ar-H), 7.40 (d, J ≈ 1.8 Hz, 1H, Ar-H), 6.96 (d, J ≈ 8.1 Hz, 1H, Ar-H), 4.17 – 4.02 (m, 4H, OCH_2), 1.95 – 1.82 (m, 2H, CH), 1.69 – 1.10 (m, 18H, CH, CH_2), 0.95 (dd, J ≈ 6.5 and J ≈ 2.3 Hz, 6H, CH_3), 0.86 (d, J ≈ 6.6 Hz, 12H, CH_3). ^{13}C NMR (125 MHz, $CDCl_3$): δ (ppm) = 191.18 (CHO), 154.79, 149.59, 110.87 (Ar-C), 129.99, 126.78, 111.77 (Ar-CH), 67.66, 67.63 (OCH_2), 39.36, 37.43, 36.15, 36.02, 24.58 (CH_2),30.11, 28.12 (CH), 22.83, 22.74, 19.83 (CH_3).

3,5-bis(dodecyloxy)benzaldehyde (2e): ($C_{31}H_{54}O_3$; 474,77 g/mol)
Yield: 19.4 g (82%), white powder. ^{1}H NMR (500 MHz, $CDCl_3$): δ (ppm) = 9.89 (s, 1H, CHO), 6.98 (d, J ≈ 2.3 Hz, 2H, Ar-H), 6.78 – 6.59 (m, 1H, Ar-H), 3.98 (t, J ≈ 6.6 Hz, 4H, OCH_2), 1.85 – 1.72 (m, 4H, CH_2), 1.56 – 1.24 (m, 36H, CH_2), 0.88 (t, J ≈ 6.9 Hz, 6H,

CH_3). ^{13}C NMR (125 MHz, $CDCl_3$): δ (ppm) = 192.29 (CHO), 160.91, 138.45 (Ar-C), 108.17, 107.74 (Ar-CH), 68.59 (OCH_2), 32.07, 29.80, 29.78, 29.74, 29.71, 29.50, 29.27, 26.14, 22.84 (CH_2), 14.27 (CH_3).

2,4-bis(dodecyloxy)benzaldehyde (2f): ($C_{31}H_{54}O_3$; 474,77 g/mol)
Yield: 18.5 g (82%), white powder. ^1H NMR (500 MHz, $CDCl_3$): δ (ppm) = 10.32 (s, 1H, CHO), 7.79 (d, J ≈ 8.7 Hz, 1H, Ar-H), 6.51 (dd, J ≈ 8.7 and J ≈ 1.7 Hz, 1H, Ar-H), 6.42 (d, J ≈ 2.1 Hz, 1H, Ar-H), 4.06 – 3.96 (m, 4H, OCH_2), 1.88 – 1.75 (m, 4H, CH_2), 1.62 – 1.25 (m, 36H, CH_2), 0.88 (t, J ≈ 6.9 Hz, 6H, CH_3). ^{13}C NMR (125 MHz, $CDCl_3$): δ (ppm) = 189.59 (CHO), 165.93, 163.53, 119.07 (Ar-C), 130.34, 106.33, 99.11 (Ar-CH), 68.63, 68.56 (OCH_2), 32.06, 29.80, 29.77, 29.73, 29.70, 29.49, 29.24, 29.17, 26.19, 26.11, 22.83 (CH_2), 14.26 (CH_3).

General Procedure for Compounds 3a-f: A solution of PPh_3 (45.6 mmol) and Zn (45.6 mmol) in dry CH_2Cl_2 (200ml) was prepared, and CBr_4 (45.6 mmol) was added. The mixture was stirred for 24h at room temperature under argon atmosphere. Then the corresponding benzaldehyde molecule **(2a-f)** (9.11mmol) was added. The reaction mixture was stirred for 24h and was filtrated through silica gel. Pure vinyl compound was isolated by column chromatography on silica gel (hexane/CH_2Cl_2 1:1).

4-(2,2-dibromovinyl)-1,2-bis(dodecyloxy)benzene (3a): ($C_{32}H_{54}Br_2O_2$; 630,59 g/mol)
Yield: 4.4 g (77%), white powder. ^1H NMR (500 MHz, $CDCl_3$): δ (ppm) = 7.38 (s, 1H, CH=CBr_2), 7.19 (d, J ≈ 2.0 Hz, 1H, Ar-H), 7.06 (dd, J ≈ 8.4 and J ≈ 1.9 Hz, 1H, Ar-H), 6.84 (d, J ≈ 8.4 Hz, 1H, Ar-H), 4.06 – 3.94 (m, 4H, OCH_2), 1.87 – 1.75 (m, 4H, CH_2), 1.59 – 1.20 (m, 36H, CH_2), 0.88 (t, J ≈ 6.9 Hz, 6H, CH_3). ^{13}C NMR (125 MHz, $CDCl_3$): δ (ppm) = 149.72, 148.73, 127.99 (Ar-C), 122.13, 113.86, 113.06 (Ar-CH), 136.68 (<u>C</u>H=CBr_2), 87.11 (CH=<u>C</u>Br_2), 69.51, 69.22 (OCH_2), 32.08, 29.85, 29.81, 29.78, 29.58, 29.55, 29.52, 29.36, 29.33, 26.16, 22.84 (CH_2), 14.27 (CH_3).

4-(2,2-dibromovinyl)-1,2-bis(tetradecyloxy)benzene (3b): ($C_{36}H_{62}Br_2O_2$; 686,70 g/mol)
Yield: 5.2 g (83%), white powder. ^1H NMR (500 MHz, $CDCl_3$): δ (ppm) = 7.38 (s, 1H, CH=CBr_2), 7.19 (d, J ≈ 1.9 Hz, 1H, Ar-H), 7.06 (dd, J ≈ 8.4 and J ≈ 1.8 Hz, 1H, Ar-H), 6.84 (d, J ≈ 8.4 Hz, 1H, Ar-H), 4.03 – 3.94 (m, 4H, OCH_2), 1.88 – 1.76 (m, 4H, CH_2), 1.57 – 1.19 (m, 44H, CH_2), 0.88 (t, J ≈ 6.9 Hz, 6H, CH_3). ^{13}C NMR (125 MHz, $CDCl_3$): δ (ppm) = 149.71, 148.73, 127.99 (Ar-C), 122.07, 113.86, 113.06 (Ar-CH), 136.68 (<u>C</u>H=CBr_2), 87.12 (CH=<u>C</u>Br_2), 69.51, 69.22 (OCH_2), 32.08, 29.96, 29.82, 29.78, 29.58, 29.55, 29.52, 29.36, 29.33, 26.17, 26.16, 22.84 (CH_2), 14.27 (CH_3).

4-(2,2-dibromovinyl)-1,2-bis(hexadecyloxy)benzene (3c): ($C_{40}H_{70}Br_2O_2$; 742,81 g/mol)
Yield: 5.4 g (80%), white powder. ^1H NMR (500 MHz, $CDCl_3$): δ (ppm) = 7.38 (s, 1H, CH=CBr_2), 7.19 (d, J ≈ 1.9 Hz, 1H, Ar-H), 7.06 (dd, J ≈ 8.4 and J ≈ 1.8 Hz, 1H, Ar-H), 6.84 (d, J ≈ 8.4 Hz, 1H, Ar-H), 4.05 – 3.93 (m, 4H, OCH_2), 1.90 – 1.74 (m, 4H, CH_2), 1.56 – 1.20 (m, 52H, CH_2), 0.88 (t, J ≈ 6.9 Hz, 6H, CH_3). ^{13}C NMR (125 MHz, $CDCl_3$): δ (ppm) = 149.72, 148.73, 127.99 (Ar-C), 122.13, 113.86, 113.06 (Ar-CH), 136.68 (<u>C</u>H=CBr_2), 87.11 (CH=<u>C</u>Br_2), 69.50, 69.22 (OCH_2), 32.09, 29.87, 29.83, 29.79, 29.78, 29.58, 29.56, 29.53, 29.37, 29.34, 26.18, 22.85 (CH_2), 14.27 (CH_3).

4-(2,2-dibromovinyl)-1,2-bis(((*S*)-3,7-dimethyloctyl)oxy)benzene (3d): ($C_{28}H_{46}Br_2O_2$; 574,48 g/mol)
Yield: 4.4 g (85%), white powder. ^1H NMR (500 MHz, $CDCl_3$): δ (ppm) = 7.39 (s, 1H, CH=CBr_2), 7.19 (d, J ≈ 2.0 Hz, 1H, Ar-H), 7.07 (dd, J ≈ 8.4 and J ≈ 2.0 Hz, 1H, Ar-H), 6.85 (d, J ≈ 8.4 Hz, 1H, Ar-H), 4.06 – 3.98 (m, 4H, OCH_2), 1.93 – 1.80 (m, 2H, CH), 1.67 – 1.11 (m, 18H, CH, CH_2), 0.94 (d, J ≈ 6.5 Hz, 6H, CH_3), 0.86 (d, J ≈ 6.6 Hz, 12H, CH_3). ^{13}C NMR (125 MHz, $CDCl_3$): δ (ppm) = 149.68, 148.70, 127.95 (Ar-C), 122.08, 113.68, 112.89 (Ar-CH), 136.68 (<u>C</u>H=CBr_2), 87.11 (CH=<u>C</u>Br_2), 67.81, 67.54 (OCH_2), 39.40, 37.47, 36.28, 36.25, 24.87 (CH_2), 30.07, 28.14 (CH), 22.86, 22.76, 19.84 (CH_3).

1-(2,2-dibromovinyl)-3,5-bis(dodecyloxy)benzene (3e): ($C_{32}H_{54}Br_2O_2$; 630,59 g/mol)
Yield: 4.3 g (76%), white powder. ^1H NMR (500 MHz, $CDCl_3$): δ (ppm) = 7.40 (s, 1H, CH=CBr_2), 6.65 (d, J ≈ 2.1 Hz, 2H, Ar-H), 6.46 – 6.41 (m, 1H, Ar-H), 3.92 (t, J ≈ 6.6 Hz, 4H, OCH_2), 1.81 – 1.71 (m, 4H, CH_2), 1.55 – 1.24 (m, 36H, CH_2), 0.88 (t, J ≈ 6.9 Hz, 6H, CH_3). ^{13}C NMR (125 MHz, $CDCl_3$): δ (ppm) = 160.27, 137.12 (Ar-C), 107.00, 102.04 (Ar-CH), 136.92 (<u>C</u>H=CBr_2), 89.80 (CH=<u>C</u>Br_2), 68.33 (OCH_2), 32.07, 29.81, 29.79, 29.75, 29.72, 29.53, 29.50, 29.34, 26.18, 22.84 (CH_2), 14.27 (CH_3).

1-(2,2-dibromovinyl)-2,4-bis(dodecyloxy)benzene (3f): ($C_{32}H_{54}Br_2O_2$; 630,59 g/mol)
Yield: 4.6 g (81%), white powder. ^1H NMR (500 MHz, $CDCl_3$): δ (ppm) = 7.69 (d, J ≈ 8.6 Hz, 1H, Ar-H), 7.55 (s, 1H, CH=CBr_2), 6.47 (dd, J ≈ 8.6 and J ≈ 2.3 Hz, 1H, Ar-H), 6.40 (d, J ≈ 2.3 Hz, 1H, Ar-H), 4.11 – 3.80 (m, 4H, OCH_2), 1.84 – 1.72 (m, 4H, CH_2), 1.54 – 1.24 (m, 36H, CH_2), 0.88 (t, J ≈ 6.9 Hz, 6H, CH_3). ^{13}C NMR (125 MHz, $CDCl_3$): δ (ppm) = 160.88, 157.61, 117.28 (Ar-C), 129.66, 104.77, 99.63 (Ar-CH), 132.47 (<u>C</u>H=CBr_2), 87.25 (CH=<u>C</u>Br_2), 68.65, 68.26 (OCH_2), 32.07, 29.82, 29.81, 29.79, 29.74, 29.72, 29.53, 29.51, 29.48, 29.39, 29.20, 26.19, 22.85 (CH_2), 14.27 (CH_3).

General Procedure for Compounds 4a-f: n-BuLi (1.6 M, 9.66 mL,14 mmol) was added slowly (over 1 h) to the corresponding dibromo alkene compound **(3a-f)** (7 mmol) in anhydrous THF (90 mL) cooled to -78 ^{o}C. The resulting brown solution was stirred at -78 ^{o}C for 1h then warmed slowly to the room temperature and stirred for a further 1 h. Saturated NH_4Cl (50 mL) was added and the mixture extracted with ether (3 x 50 mL). The combined organic extracts were dried over $MgSO_4$ and concentrated in vacuo. The residue was purified by column chromatography (silica gel, eluent hexane/ethyl acetate 10:1).

1,2-bis(dodecyloxy)-4-ethynylbenzene (4a): ($C_{32}H_{54}O_2$; 470,78 g/mol)
Yield: 2.7 g (84%), white powder. ^{1}H NMR (500 MHz, $CDCl_3$): δ (ppm) = 7.05 (dd, J ≈ 8.3 Hz and J ≈ 1.9 Hz, 1H, Ar-H), 6.99 (d, J ≈ 1.9 Hz, 1H, Ar-H), 6.79 (d, J ≈ 8.3 Hz,1H, Ar-H), 4.06 - 3.89 (m, 4H, 2 OCH_2), 2.98 (s, 1H, C≡CH), 1.86 – 1.76 (m, 4H, CH_2), 1.55-1.24 (m, 36H, CH_2), 0.88 (t, J ≈ 6.9 Hz, 6H, CH_3). ^{13}C NMR (125 MHz, $CDCl_3$): δ (ppm) = 150.23, 148.80, 117.28 (Ar-C), 125.65, 114.19, 113.26 (Ar-CH), 84.13 (C≡CH), 75.55 (C≡CH), 69.40, 69.27 (OCH_2), 32.08, 29.85, 29.81, 29.77, 29.55, 29.52, 29.33, 29.31, 26.14, 22.85 (CH_2), 14.27 (CH_3).
4-ethynyl-1,2-bis(tetradecyloxy)benzene (4b): ($C_{36}H_{62}O_2$; 526,89 g/mol)
Yield: 3.0 g (80%), white powder. ^{1}H NMR (500 MHz, $CDCl_3$): δ (ppm) = 7.06 (dd, J ≈ 8.3 Hz and J ≈ 1.8 Hz, 1H, Ar-H), 6.99 (d, J ≈ 1.7 Hz, 1H, Ar-H), 6.79 (d, J ≈ 8.3 Hz, 1H, Ar-H), 4.04 - 3.88 (m, 4H, OCH_2), 2.98 (s, 1H, C≡CH), 1.87 – 1.75 (m, 4H, CH_2), 1.58-1.21 (m, 44H, CH_2), 0.88 (t, J ≈ 6.9 Hz, 6H, CH_3). ^{13}C NMR (125 MHz, $CDCl_3$): δ (ppm) = 150.23, 148.80, 117.27 (Ar-C), 125.65, 114.19, 113.25 (Ar-CH), 84.13 (C≡CH), 75.55 (C≡CH), 69.40, 69.27 (OCH_2), 32.08, 29.86, 29.82, 29.77, 29.55, 29.52, 29.33, 29.31, 26.14, 22.84 (CH_2), 14.27 (CH_3).

4-ethynyl-1,2-bis(hexadecyloxy)benzene (4c): ($C_{40}H_{70}O_2$; 583,00 g/mol)
Yield: 3.3 g (82%), white powder. ^{1}H NMR (500 MHz, $CDCl_3$): δ (ppm) = 7.06 (dd, J ≈ 8.3 Hz and J ≈ 1.8 Hz, 1H, Ar-H), 6.99 (d, J ≈ 1.7 Hz, 1H, Ar-H), 6.79 (d, J ≈ 8.3 Hz, 1H, Ar-H), 4.04 - 3.88 (m, 4H, OCH_2), 2.98 (s, 1H, C≡CH), 1.87 – 1.75 (m, 4H, CH_2), 1.58 - 1.21 (m, 44H, CH_2), 0.88 (t, J ≈ 6.9 Hz, 6H, CH_3). ^{13}C NMR (125 MHz, $CDCl_3$): δ (ppm) = 150.23, 148.80, 117.28 (Ar-C), 125.66, 114.19, 113.26 (Ar-CH), 84.13 (C≡CH), 75.55 (C≡CH), 69.40, 69.27 (OCH_2), 32.08, 29.87, 29.82, 29.78, 29.55, 29.52, 29.33, 29.31, 26.14, 22.85 (CH_2), 14.27 (CH_3).

1,2-bis(((*S*)-3,7-dimethyloctyl)oxy)-4-ethynylbenzene (4d): ($C_{28}H_{46}O_2$; 414,67 g/mol)
Yield: 2.3 g (80%), white powder. ^{1}H NMR (500 MHz, $CDCl_3$): δ (ppm) = 7.06 (dd, J ≈ 8.3 Hz and J ≈ 1.9 Hz, 1H, Ar-H), 6.99 (d, J ≈ 1.8 Hz, 1H, Ar-H), 6.79 (d, J ≈ 8.3 Hz, 1H, Ar-H), 4.06 - 3.98 (m, 4H, OCH_2), 2.98 (s, 1H, C≡CH), 1.93 – 1.80 (m, 2H, CH), 1.71 - 1.11 (m, 18H, CH, CH_2), 0.94 (t, J ≈ 6.9 Hz, 6H, CH_3), 0.87 (dd, J ≈ 6.6 Hz, 12H, CH_3). ^{13}C NMR (125 MHz, $CDCl_3$): δ (ppm) = 150.20, 148.79, 117.09 (Ar-C), 125.62, 114.16, 113.11 (Ar-CH), 84.14 (C≡CH), 75.56 (C≡CH), 67.72, 67.61 (OCH_2), 39.39, 37.47, 36.26, 36.23, 24.86 (CH_2), 30.07, 28.13 (CH), 22.85, 22.75, 19.84 (CH_3).

1,3-bis(dodecyloxy)-5-ethynylbenzene (4e): ($C_{32}H_{54}O_2$; 470,78 g/mol)
Yield: 5.46 g (78%), white powder. ^{1}H NMR (500 MHz, $CDCl_3$): δ (ppm) = 6.62 (d, J ≈ 2.3, 2H, Ar-H), 6.52 – 6.39 (m, 1H, Ar-H), 3.91 (t, J ≈ 6.6 Hz, 4H, OCH_2), 3.01 (s, 1H, C≡CH), 1.79 – 1.70 (m, 4H, CH_2), 1.57 - 1.24 (m, 36H, CH_2), 0.88 (t, J ≈ 6.9 Hz, 6H, CH_3). ^{13}C NMR (125 MHz, $CDCl_3$): δ (ppm) = 160.17, 123.29 (Ar-C), 110.54, 103.31 (Ar-CH), 83.94 (C≡CH), 76.57 (C≡CH), 68.33 (OCH_2), 32.07, 29.81, 29.78, 29.74, 29.72, 29.50, 29.31, 26.15, 22.84 (CH_2), 14.27 (CH_3).

2,4-bis(dodecyloxy)-1-ethynylbenzene (**4f**): ($C_{32}H_{54}O_2$; 470,78 g/mol)
Yield: 2.8 g (85%), white powder. ^{1}H NMR (500 MHz, $CDCl_3$): δ (ppm) = 7.34 (dd, J ≈ 8.3 Hz and J ≈ 1.8 Hz, 1H, Ar-H), 6.43 - 6.37 (m, 2H, Ar-H), 4.01 - 3.90 (m, 4H, OCH_2), 3.17 (s, 1H, C≡CH), 1.86 – 1.72 (m, 4H, 2 CH_2), 1.57 - 1.24 (m, 36H, CH_2), 0.88 (t, J ≈ 7.0 Hz, 6H, CH_3). ^{13}C NMR (125 MHz, $CDCl_3$): δ (ppm) = 161.61, 161.10, 104.03 (Ar-C), 134.90, 105.49, 100.01 (Ar-CH), 80.47 (C≡CH), 79.49 (C≡CH), 68.91, 68.32 (OCH_2), 32.07, 29.81, 29.79, 29.74, 29.71, 29.53, 29.50, 29.35, 29.15, 26.16, 26.06, 22.84 (CH_2), 14.27 (CH_3).

General Procedure for Compounds 5a-f: $PdCl_2(PPh_3)_2$ (0.02 mmol), *p*-bromobenzaldehyde (2.0 mmol), H_2O (2.5 mL), and triethylamine (10 mmol) were added to a round-bottom reaction flask, and the resulting mixture was stirred at 50 °C for 5 min. Then the corresponding acetylenic compound **(4a-f)** was added (2.4 mmol), and the reaction mixture was stirred at 50 °C for 24 h. After extraction with EtOAc (3x10 mL), the combined organic layers were dried with anhydrous sodium sulphate. The solvent was removed under vacuum, and the residue was purified by column chromatography (silica gel, H / EA 4:1) to give the desired product.

4-((3,4-bis(dodecyloxy)phenyl)ethynyl)benzaldehyde (5a): ($C_{39}H_{58}O_3$; 574,89 g/mol)
Yield: 0.55 g (48%), white powder. ^{1}H NMR (500 MHz, $CDCl_3$): δ (ppm) = 10.01 (s, 1H, CHO), 7.85 (d, J ≈ 8.2 Hz, 2H, Ar-H), 7.65 (d, J ≈ 8.1 Hz, 2H, Ar-H), 7.12 (dd, J ≈ 8.3 Hz and J ≈ 1.7 Hz, 1H, Ar-H), 7.05 (d, J ≈ 1.7 Hz; 1H, Ar-H), 6.84 (d, J ≈ 8.3 Hz,

1H, Ar-H), 4.17-3.91 (m, 4H, OCH_2), 1.88 – 1.78 (m, 4H, CH_2), 1.58-1.23 (m, 36H, CH_2), 0.88 (t, J ≈ 6.7 Hz, 6H, CH_3). ^{13}C NMR (125 MHz, $CDCl_3$): δ (ppm) = 191.59 (CHO), 150.48, 148.94, 135.26, 130.20, 114.55 (Ar-C), 132.03, 129.74, 125.51, 116.84, 113.29 (Ar-CH), 94.30 (C≡C), 87.32 (C≡C), 69.46, 69.28 (OCH_2), 32.08, 29.85, 29.81, 29.78, 29.77, 29.56, 29.52,29.35, 29.31, 29.16, 26.15, 22.84 (CH_2), 14.27 (CH_3).

4-((3,4-bis(tetradecyloxy)phenyl)ethynyl)benzaldehyde (5b): ($C_{43}H_{66}O_3$; 631,00 g/mol)
Yield: 0.63 g (50%), white powder. ^{1}H NMR (500 MHz, $CDCl_3$): δ (ppm) = 10.01 (s, 1H, CHO), 7.85 (d, J ≈ 8.3 Hz, 2H, Ar-H), 7.65 (d, J ≈ 8.2 Hz, 2H, Ar-H), 7.12 (dd, J ≈ 8.3 Hz and J ≈ 1.9 Hz, 1H, Ar-H), 7.05 (d, J ≈ 1.8 Hz, 1H, Ar-H), 6.84 (d, J ≈ 8.3 Hz, 1H, Ar-H), 4.06-3.97 (m, 4H, OCH_2), 1.90 – 1.76 (m, 4H, CH_2), 1.60 - 1.22 (m, 44H, CH_2), 0.87 (t, J ≈ 6.8 Hz, 6H, CH_3). ^{13}C NMR (125 MHz, $CDCl_3$): δ (ppm) = 191.61 (CHO), 150.46, 148.91, 135.24, 130.19, 114.53 (Ar-C), 132.03, 129.74, 125.50, 116.79, 113.25 (Ar-CH), 94.30 (C≡C), 87.31 (C≡C), 69.43, 69.25 (OCH_2), 32.08, 29.86, 29.82, 29.78, 29.55, 29.52, 29.34, 29.30, 26.14, 22.84 (CH_2), 14.27 (CH_3).

4-((3,4-bis(hexadecyloxy)phenyl)ethynyl)benzaldehyde (5c): ($C_{47}H_{74}O_3$; 687,11 g/mol)
Yield: 0.41 g (30%), white powder. ^{1}H NMR (500 MHz, $CDCl_3$): δ (ppm) = 10.01 (s, 1H, CHO), 7.85 (d, J ≈ 8.3 Hz, 2H, Ar-H), 7.65 (d, J ≈ 8.2 Hz, 2H, Ar-H), 7.13 (dd, J ≈ 8.3 Hz and J ≈ 1.9 Hz, 1H, Ar-H), 7.05 (d, J ≈ 1.9 Hz; 1H, Ar-H), 6.84 (d, J ≈ 8.3 Hz, 1H, Ar-H), 4.05 - 3.97 (m, 4H, OCH_2), 1.89 – 1.76 (m, 4H, CH_2), 1.60 - 1.17 (m, 44H, CH_2), 0.87 (t, J ≈ 6.9 Hz, 6H, CH_3). ^{13}C NMR (125 MHz, $CDCl_3$): δ (ppm) = 191.61 (CHO), 150.46, 148.91, 135.24, 130.19, 114.53 (Ar-C), 132.03, 129.74, 125.50, 116.79, 113.25 (Ar-CH), 94.30 (C≡C), 87.31 (C≡C), 69.43, 69.25 (OCH_2), 32.08, 29.87,29.82, 29.79, 29.78, 29.56, 29.52, 29.35, 29.30, 26.14, 22.85 (CH_2), 14.28 (CH_3).

4-((3,4-bis(((*S*)-3,7-dimethyloctyl)oxy)phenyl)ethynyl)benzaldehyde (5d): ($C_{35}H_{50}O_3$; 518,78 g/mol)
Yield: 0.6 g (57%), white powder. ^{1}H NMR (500 MHz, $CDCl_3$): δ (ppm) = 10.01 (s, 1H, CHO), 7.85 (d, J ≈ 8.1 Hz, 2H, Ar-H), 7.65 (d, J ≈ 8.1 Hz, 2H, Ar-H), 7.13 (dd, J ≈ 8.3 Hz and J ≈ 1.7 Hz, 1H, Ar-H), 7.06 (d, J ≈ 1.7 Hz, 1H, Ar-H), 6.85 (d, J ≈ 8.3 Hz, 1H, Ar-H), 4.11 - 3.99 (m, 4H, OCH_2), 1.95 – 1.83 (m, 2H, CH), 1.75 - 1.10 (m, 18H, CH, CH_2) 0.94 (t, J ≈ 6.9 Hz, 6H, CH_3), 0.87 (d, J ≈ 6.6 Hz, 12H, CH_3). ^{13}C NMR (125 MHz, $CDCl_3$): δ (ppm) = 191.59 (CHO), 150.45, 148.94, 135.26, 130.19, 114.52 (Ar-C), 132.03, 129.74, 125.48, 116.66, 113.15 (Ar-CH), 94.30 (C≡C), 87.33 (C≡C), 67.78, 67.62 (OCH_2), 39.39, 37.48, 36.29, 36.23, 24.87 (CH_2), 30.09, 28.14 (CH), 22.85, 22.76, 19.86 (CH_3).

4-((3,5-bis(dodecyloxy)phenyl)ethynyl)benzaldehyde (5e): ($C_{39}H_{58}O_3$; 574,89 g/mol)
Yield: 0.58 g (51%), white powder. ^{1}H NMR (500 MHz, $CDCl_3$): δ (ppm) = 10.02 (s, 1H, CHO), 7.86 (d, J ≈ 8.3 Hz, 2H, Ar-H), 7.66 (d, J ≈ 8.2 Hz, 2H, Ar-H), 6.68 (d, J ≈ 2.2 Hz, 2H, Ar-H), 6.52 – 6.43 (m, 1H, Ar-H), 3.95 (t, J ≈ 6.6 Hz, 4H, OCH_2), 1.82 – 1.69 (m, 4H, CH_2), 1.59 - 1.22 (m, 36H, CH_2) 0.88 (t, J ≈ 6.9 Hz, 6H, CH_3). ^{13}C NMR (125 MHz, $CDCl_3$): δ (ppm) = 191.59 (CHO), 135.54, 123.67, 103.50 (Ar-C), 160.30, 132.28, 129.72, 110.16 (Ar-CH), 93.83 (C≡C), 87.96 (C≡C), 68.39 (OCH_2), 32.07, 29.81, 29.79, 29.74, 29.72, 29.51, 29.33, 26.16, 22.84 (CH_2), 14.27 (CH_3).

4-((2,4-bis(dodecyloxy)phenyl)ethynyl)benzaldehyde (5f): ($C_{39}H_{58}O_3$; 574,89 g/mol)
Yield: 0.6 g (53%), white powder. ^{1}H NMR (500 MHz, $CDCl_3$): δ (ppm) = 10.00 (s, 1H, CHO), 7.83 (d, J ≈ 8.3 Hz, 2H, Ar-H), 7.63 (d, J ≈ 8.2 Hz, 2H, Ar-H), 7.40 (d, J ≈ 8.3, 1H, Ar-H), 6.47 (dd, J ≈ 8.4 and J ≈ 2.3 Hz; 1H, Ar-H), 6.45 (d, J ≈ 2.1 Hz, 1H, Ar-H), 4.07 - 3.91 (m, 4H, OCH_2), 1.93 – 1.75 (m, 4H, CH_2), 1.60 - 1.20 (m, 36H, CH_2), 0.87 (t, J ≈ 6.9 Hz, 6H, CH_3). ^{13}C NMR (125 MHz, $CDCl_3$): δ (ppm) = 191.62 (CHO), 161.55, 161.43, 134.98, 130.88, 104.48 (Ar-C), 134.34, 131.84, 129.70, 105.79, 100.00 (Ar-CH), 91.57 (C≡C), 91.16 (C≡C), 68.83, 68.40 (OCH_2), 32.07, 29.84, 29.82, 29.79, 29.77, 29.75, 29.72, 29.56, 29.53, 29.50, 29.35, 29.32, 26.22, 26.17, 22.84 (CH_2), 14.27 (CH_3).

General Procedure For Compounds 6a-f: Corresponding aldehyde derivatives (**5a-f**) (0.8 mmol) and 4,4',6,6'-tetramethyl-[2,2']-bipyrimidine (**1**) were added to an aqueous sodium hydroxide solution (5 M, 15 mL) containing Aliquat 336 and the mixture was heated under reflux for 72h. After extraction three times with CH_2Cl_2, the combined organic phases were washed with saturated NaCl solution and dried over $MgSO_4$. The solvents were evaporated and the residues were purified by column chromatography (silica gel, CH_2Cl_2). And the last procedure is recrystallization from a CH_2Cl_2 / MeOH.

4,4',6,6'-tetrakis((E)-4-((3,4-bis(dodecyloxy)phenyl)ethynyl)styryl)-2,2'-bipyrimidine (6a): ($C_{168}H_{238}N_4O_8$; 2441,77g/mol)
Yield: 0.091 g (20%), yellow powder. ^{1}H NMR (500 MHz, $CDCl_3$): δ (ppm) = 8.01 (d, J ≈ 16.0 Hz, 4H, C=CH), 7.64 (d, J ≈ 8.1 Hz, 8H, Ar-H), 7.59 (s, 2H, Ar(N)-H), 7.56 (d, J ≈ 8.0 Hz, 8H, Ar-H), 7.34 (d, J ≈ 16.0 Hz, 4H, C=CH), 7.12 (d, J ≈ 8.2 Hz, 4H, Ar-H), 7.06 (d, J ≈ 1.8 Hz, 4H, Ar-H), 6.84 (d, J ≈ 8.4 Hz, 4H, Ar-H), 4.07 - 3.98 (m, 16H, OCH_2), 1.87 – 1.79 (m, 16H, CH_2), 1.59-1.21 (m, 144H, CH_2), 0.88 (t, J ≈ 6.5 Hz, 24H, CH_3). ^{13}C NMR (125 MHz, $CDCl_3$): δ (ppm) = 163.98, 150.10, 148.93, 135.28, 115.21 (Ar-C), 132.10, 128.05, 128.03, 128.01, 125.28, 116.81, 113.39 (Ar-CH, C=CH), 87.98 (C≡C), 69.44, 69.31 (OCH_2), 32.08,

29.86, 29.82, 29.79, 29.78, 29.58, 29.53, 29.39, 29.35, 26.19, 26.16, 22.85 (CH_2), 14.27 (CH_3). Anal. Found: C, 78.87; H, 9.76; N, 1.90. $C_{168}H_{238}N_4O_8$ calc.: C, 82.64; H, 9.82; N, 2.29. LC-MS (ESI): m/z 2442.251 ($[M^+H]^+$) $C_{168}H_{238}N_4O_8$ requires 2439.83.

4,4',6,6'-tetrakis((E)-4-((3,4-bis(tetradecyloxy)phenyl)ethynyl)styryl)-2,2'-bipyrimidine (6b): ($C_{184}H_{270}N_4O_8$; 2664,08 g/mol)
Yield: 0.11 g (22%), yellow powder. ^{1}H NMR (500 MHz, $CDCl_3$): δ (ppm) = 8.01 (d, J ≈ 16.1 Hz, 4H, C=CH), 7.65 (d, J ≈ 8.4 Hz, 8H, Ar-H), 7.59 (s, 2H, Ar(N)-H), 7.56 (d, J ≈ 8.2 Hz, 8H, Ar-H), 7.34 (d, J ≈ 16.1 Hz, 4H, C=CH), 7.12 (dd, J ≈ 8.2 and J ≈ 1.8 Hz, 4H, Ar-H), 7.06 (d, J ≈ 1.8 Hz, 4H, Ar-H), 6.84 (d, J ≈ 8.4 Hz, 4H, Ar-H), 4.05 - 3.96 (m, 16H, OCH_2), 1.90 – 1.77 (m, 16H, CH_2), 1.63-1.20 (m, 176H, CH_2), 0.88 (t, J ≈ 6.9 Hz, 24H, CH_3). ^{13}C NMR (125 MHz, $CDCl_3$): δ (ppm) = 164.05, 150.07, 148.92, 135.43, 124.80, 115.21 (Ar-C), 137.02, 132.08, 127.80, 127.13, 125.25, 116.81, 113.40 (Ar-CH, C=CH), 91.93, 87.93 (C≡C), 69.44, 69.31 (OCH_2), 32.08, 29.86, 29.82, 29.78, 29.57, 29.52, 29.38, 29.34, 26.18, 26.16, 22.85 (CH_2), 14.27 (CH_3). Anal. Found: C, 79.70 H, 10.32; N, 1.80. $C_{184}H_{270}N_4O_8$ calc.: C, 82.89; H, 10.21; N, 2.10. LC-MS (ESI): m/z 2667.874 ($[M^+H]^+$) $C_{184}H_{270}N_4O_8$ requires 2664.08.

4,4',6,6'-tetrakis((E)-4-((3,4-bis(hexadecyloxy)phenyl)ethynyl)styryl)-2,2'-bipyrimidine (6c): ($C_{200}H_{302}N_4O_8$; 2890,64 g/mol)
Yield: 0.097 g (18%), yellow powder. ^{1}H NMR (500 MHz, $CDCl_3$): δ (ppm) = 8.01 (d, J ≈ 16.0 Hz, 4H, C=CH), 7.65 (d, J ≈ 8.4 Hz, 8H, Ar-H), 7.59 (s, 2H, Ar(N)-H), 7.56 (d, J ≈ 8.1 Hz, 8H, Ar-H), 7.34 (d, J ≈ 16.0 Hz, 4H, C=CH), 7.12 (dd, J ≈ 8.2 and J ≈ 1.8 Hz, 4H, Ar-H), 7.06 (d, J ≈ 1.8 Hz, 8H, Ar-H), 6.84 (d, J ≈ 8.4 Hz, 4H, Ar-H), 4.05 - 3.95 (m, 16H, OCH_2), 1.87 – 1.77 (m, 16H, CH_2), 1.57 - 1.22 (m, 208 H, CH_2), 0.87 (t, J ≈ 6.9 Hz, 24H, CH_3). ^{13}C NMR (125 MHz, $CDCl_3$): δ (ppm) = 164.05, 150.04, 148.89, 135.42, 124.78, 115.22 (Ar-C), 137.00, 132.07, 127.80, 127.12, 125.23, 116.76, 113.35 (Ar-CH, C=CH), 91.92, 87.93 (C≡C), 69.41, 69.29 (OCH_2), 32.07, 29.85, 29.78, 29.74, 29.56, 29.50, 29.36, 29.33, 26.17, 26.15, 22.84 (CH_2), 14.27 (CH_3). Anal. Found: C, 80.98; H, 10.72; N, 1.63. $C_{200}H_{302}N_4O_8$ calc.: C, 83.10; H, 10.53; N, 1.94. LC-MS (ESI): m/z 2891.890 ($[M^+H]^+$), $C_{200}H_{302}N_4O_8$ requires 2888.33.

4,4',6,6'-tetrakis((E)-4-((3,4-bis(((*S*)-3,7-dimethyloctyl)oxy)phenyl)ethynyl)styryl)-2,2'-bipyrimidine (6d): ($C_{152}H_{206}N_4O_8$; 2217,34 g/mol)
Yield: 0.087 g (21%), yellow powder. ^{1}H NMR (500 MHz, $CDCl_3$): δ (ppm) = 8.01 (d, J ≈ 16.0 Hz, 4H, C=CH), 7.65 (d, J ≈ 8.4 Hz, 8H, Ar-H), 7.59 (s, 2H, Ar(N)-H), 7.57 (d, J ≈ 8.3 Hz, 8H, Ar-H), 7.35 (d, J ≈ 16.0 Hz, 4H, C=CH), 7.12 (dd, J ≈ 8.2 and J ≈ 1.8 Hz, 4H, Ar-H), 7.06 (d, J ≈ 1.8 Hz, 4H, Ar-H), 6.85 (d, J ≈ 8.4 Hz, 4H, Ar-H), 4.11 - 3.99 (m, 16H, OCH_2), 1.94 – 1.83 (m, 8H, CH_2), 1.68 - 1.17 (m, 72 H, CH, CH_2), 0.96 (dd, J ≈ 6.5 and J ≈ 2.3 Hz, 24H, CH_3), 0.87 (d, J ≈ 6.6 Hz, 12H, CH_3). ^{13}C NMR (125 MHz, $CDCl_3$): δ (ppm) = 164.05, 150.01, 148.89, 135.42, 124.78, 115.19 (Ar-C), 137.00, 132.08, 127.80, 127.12, 125.20, 116.58, 113.21 (Ar-CH, C=CH), 91.93, 87.93 (C≡C), 67.73, 67.63 (OCH_2), 39.41, 39.40, 37.49, 36.30, 36.25, 24.87 (CH_2), 30.08, 28.14 (CH), 22.86, 22.76 19.86 (CH_3). Anal. Found: C, 80.67; H, 9.67; N, 2.26. $C_{152}H_{206}N_4O_8$ calc.: C, 82.34; H, 9.36; N, 2.53. LC-MS (ESI): m/z 2217.111 ($[M^+H]^+$), $C_{152}H_{206}N_4O_8$ requires 2215.58.

4,4',6,6'-tetrakis((E)-4-((3,5-bis(dodecyloxy)phenyl)ethynyl)styryl)-2,2'-bipyrimidine (6e): ($C_{168}H_{238}N_4O_8$; 2441,77 g/mol)
Yield: 0.10 g (22%), yellow powder. ^{1}H NMR (500 MHz, $CDCl_3$): δ (ppm) = 8.01 (d, J ≈ 16.1 Hz, 4H, C=CH), 7.65 (d; J ≈ 8.4 Hz, 8H, Ar-H), 7.60 (s, 2H, Ar(N)-H), 7.58 (d, J ≈ 8.3 Hz, 8H, Ar-H), 7.35 (d, J ≈ 16.1 Hz, 4H, C=CH), 6.69 (d, J ≈ 2.2 Hz, 8H, Ar-H), 6.49 – 6.45 (m, 8H, Ar-H), 3.95 (t, J ≈ 6.5 Hz, 16H, OCH_2), 1.83 – 1.74 (m, 16H, CH_2), 1.61 -1.22 (m, 144H, CH_2), 0.88 (t, J ≈ 6.9 Hz, 24H, CH_3). ^{13}C NMR (125 MHz, $CDCl_3$): δ (ppm) = 160.24, 135.75, 124.38, 124.27 (Ar-C), 136.95, 132.29, 127.80, 127.29, 110.03, 103.08 (Ar-CH, C=CH), 91.67, 88.75 (C≡C), 68.35 (OCH_2), 32.07, 29.84, 29.81, 29.79, 29.75, 29.73, 29.52, 29.50, 29.35, 26.17, 22.84 (CH_2), 14.27 (CH_3). Anal. Found: C, 80.34; H, 10.21; N, 1.78. $C_{168}H_{238}N_4O_8$ calc.: C, 82.64; H, 9.82; N, 2.29. LC-MS (ESI): m/z 2442.597 ($[M^+H]^+$), $C_{168}H_{238}N_4O_8$ requires 2439.83).

4,4',6,6'-tetrakis((E)-4-((2,4-bis(dodecyloxy)phenyl)ethynyl)styryl)-2,2'-bipyrimidine (6f): ($C_{168}H_{238}N_4O_8$; 2441,77 g/mol)
Yield: 0.09 g (20%), yellow powder. ^{1}H NMR (500 MHz, $CDCl_3$): δ (ppm) = 7.92 (d, J ≈ 16.1 Hz, 4H, C=CH), 7.56 (d, J ≈ 8.4 Hz, 8H, Ar-H), 7.51 (s, 2H, Ar(N)-H), 7.48 (d, J ≈ 8.3 Hz, 8H, Ar-H), 7.33 (d, J ≈ 8.1 Hz, 4H, Ar-H), 7.26 (d, J ≈ 16.1 Hz, 4H, C=CH), 6.43 – 6.37 (m, 8H, Ar-H), 4.14 - 3.86 (m, 16H, OCH_2), 1.91 – 1.74 (m, 16H, CH_2), 1.58-1.24 (m, 144H, CH_2), 0.87 (t, J ≈ 6.5 Hz, 24H, CH_3). ^{13}C NMR (125 MHz, $CDCl_3$): δ (ppm) = 164.05, 150.07, 148.95, 135.43, 124.80, 115.21 (Ar-C), 137.02, 132.08, 127.80, 127.07, 125.25, 116.81, 113.40 (Ar-CH, C=CH), 91.96, 87.93 (C≡C), 69.44, 69.31 (OCH_2), 32.08, 29.96, 29.82, 29.78, 29.57, 29.52, 29.38, 29.34, 26.18, 26.11, 22.85 (CH_2), 14.27 (CH_3). Anal. Found: C, 80.31; H, 10.28; N, 0.65. $C_{168}H_{238}N_4O_8$ calc.: C, 82.64; H, 9.82; N, 2.29. LC-MS (ESI): m/z 2442.572 ($[M^+H]^+$), $C_{168}H_{238}N_4O_8$ requires 2439.83.

Acknowledgements

This research has been supported by The Scientific and Technological Research Council of Turkey (TÜBİTAK), in the framework of TÜBİTAK-2232 program (Project Number 118C273).

Conflicts of Interest

The authors declare no conflict of interest.

Entry for the Table of Contents

Smart design of 3D π-conjugated octupolar organic materials with self-organizing properties which allows the emergence of highly luminescent multifunctional liquid crystalline chromophores exhibiting quantum yields and displaying very good second and cubic NLO activities. The crucial efficient transfer of chirality from molecule to supramolecular material lead to non-centrosymmetric organization resulting in a strong Second Harmonic Generation at the solid state.

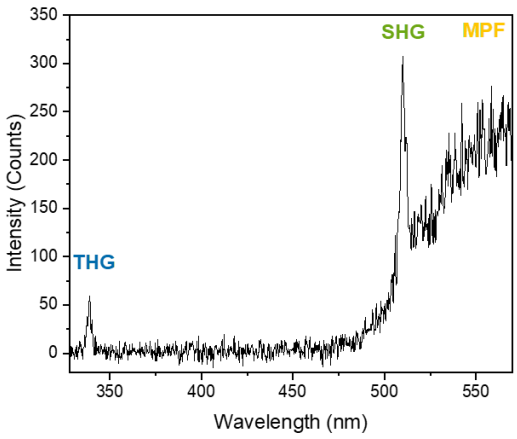

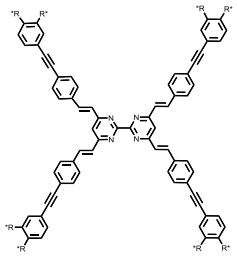

@YildizEdu, @chimie_ISCR, @science@leuven, @UHA68, @AkdasKilic,

[1] H. K. Bisoyi, Q. Li, *Chem.Rev.* **2022**, 122, 4887−4926.

[2] [a] P. G. De Gennes, J. Prost, *The physics of liquid crystals* **1995**, Oxford University Press; [b] M. Kléman, O. D. Lavrentovich, *Soft matter physics: an introduction* **2003**, New York: Springer; [c] J. Li, W. Y. Wong, X. M. Tao, *Nanoscale* **2020**,12, 1281−1306.

[3] [a] I. Dierking, *Textures of Liquid Crystals* **2003,** Weinheim: John Wiley & Sons; [b] P. J. Ackerman, I. I. Smalyukh, *Nat. Mater.* **2017**, 16, 426–432; [c] Y. Xia, T. S. Mathis, M. Q. Zhao, B. Anasori, A. Dang, Z. Zhou, H. Cho, Y. Gogotsi, S. Yang, *Nature* **2018**, 557, 409–412; [d] J. Xiong, Q. Yang, Y. Li, S. T. Wu., *Light Sci. Appl.* **2022**, 11, 54-63; [e] T. Badloe, J. Kim, I. Kim, W. S. Kim, W. S. Kim, *Light Sci. Appl.* **2022**, 11, 118-129; [f] L. L. Ma, C. Liu, S.-B. Wu, P. Chen, Q.-M. Chen, J.-X. Qian, S.-J. Ge, Y.-H. Wu, W. Hu, Y.-Q. Lu, *Sci. Adv.* **2021**, 7; [g] K. J. Ihn, R. Pindak, J. A. Zasadzinski, A. J. Slaney, J. Goodby, *Science* **1992**, 258, 275–278.

[4] [a] E.-L. Hsiang, Z. Yang, Q. Yang, Y.-F. Lan, S.-T. Wu, *J. Soc. Inf. Disp.* **2021**, 29, 446−465; [b] Y. Huang, E.-H. Hsiang, M.-Y. Deng, S.-T. Wu, *Light Sci. Appl.* **2020**,9, 105-121.

[5] [a] P. Popov, E.K. Mann, A. Jakli, *J. Mater. Chem. B* **2017**, 5, 5061–5078; [b] W. Shin, T. Yasuda, G. Watanabe, Y.S. Yang, C. Adachi, *Chem. Mater.* **2013**, 25, 2549–2556; [c] M.P. Aldred, A.E.A. Contoret, S.R. Farrar, S.M. Kelly, D. Mathieson, M. O'Neill, C.W. Tsoi, P. Vlachos, *Adv. Mater.* **2005**, 17, 1368–1372; [d] J.P.F. Lagerwall, G. Scalia, *J Mater Sci: Mater Electron* **2021**, 32, 28870–28881.

[6] [a] C. Ma, W. Lu, X. Yang, J. He, X. Le, L. Wang, J. Zhang, M.J. Serpe, Y. Huang, T. Chen, *Adv. Funct. Mater.* **2018**, 28, 1704568; [b] S. Diring, F. Camerel, B. Donnio, T. Dintzer, S. Toffanin, R. Capelli, M. Muccini, R. Ziessel, *J. Am. Chem. Soc.* **2009**, 131, 18177–18185; [c] R. Forschner, J. A. Knöller, A. Zens, W. Frey, Y. Molard, S. Laschat, *Liquid Crystals* **2023**, Print Online; [c] L. Zhang, Y. Cui, Q. Wang, H. Zhou, H. Wang, Y. Li, Z. Yang, H. Cao, D. Wang, W. He, *Molecules* **2022**, 27, 5536.

[7] [a] J. Zyss, *Ed. Molecular Nonlinear Optics: Materials, Physics and DeVices* **1994**, Academic Press: Boston; [b] Nalwa, H. S., Miyata, S., *Eds. Nonlinear Optics of Organic Molecules and Polymers* **1994**, CRC Press: Boca Raton, FL; [c] P. N. Prasad, D. J. William, *Introduction to Nonlinear Optical Effects in Molecules and Polymers* **1991**, John Wiley: New York; [d] G. A. Lindsay, K. D. Singer, *Polymers for Second-order Nonlinear Optics; ACS Symposium Series 601* **1994**, American Chemical Society: Washington, DC. [e] L. R. Dalton, A. W. Harper, R. Ghosn, W. H. Steier, M. Ziari, H. Fetterman, Y. Shi, R. V. Mustacich, A. K. Y. Jen, K. J. Shea, *Chem. ReV.* **1995**, 7, 1060; [f] Z. Cheng, L. R. Dalton, M.-C. Oh, Z. Hua, W. H. Steier, *Chem. Mater.* **2001**, 13 (9), 3043-3050.

[8] J. Zyss and I. Ledoux, *Chem. Rev.* **1994**, 94, 77-105; [b] S. Bidault, S. Brasselet, and J. Zyss, O. Maury and H. Le Bozec, *The J. of Chem. Phys.* 2007, 126, 034312.

[9] [a] D. N. Nikogosyan, *Nonlinear optical crystals: A complete survey* **2005**, Springer Science, New York; [b] C. T. Chen, T. Sasaki, R. K. Li, Y. C. Wu, Z. S. Lin and Y. Mori, *Nonlinear optical borate crystals: Principals and applications* 2012, John Wiley & Sons; [c] S. L. Pan, Y. Wang and K. R. Poeppelmeier, *Photonic and Electronic Properties of Fluoride Materials* **2016**, 311–354, ed. A. Tressaud and K. Poeppelmeier, Elsevier, Boston; [d] H. Liu, B. Zhang, Y. Wang, *Chem. Commun.* **2020**, 56, 13689-13701.

[10] A. Amar, A. ElKechai, J.-F. Halet, F. Paul, A. Boucekkine, *New J. Chem.* **2021**, 45, 15074–15081.

[11] H. Akdas-Kilig , T. Roisnel , I. Ledoux and H. Le Bozec , *New J. Chem.* **2009**, 33 , 1470 —1473.

[12] M. Feckova, P. Le Poul, F. Bures, F. Robin-le Guen, S. Achelle, *Dyes and Pigments* **2020**, 182, 108659.

[13] [a] H. Akdas-Kilig, M. Godfroy, J.-L. Fillaut, B. Donnio, B. Heinrich, P. Kędziora, J.-P. Malval, A. Spangenberg, S. van Cleuvenbergen, K. Clays, and F. Camerel, *J. Phys. Chem. C* **2015**, 119(7), 3697–3710; [b] S. van Cleuvenbergen, P. Kędziora, J.-L. Fillaut, T. Verbiest, K. Clays, H. Akdas-Kilig, F. Camerel, *Angew. Chem. Int. Ed*. **2017**, 56(32), 9546–9550.

[14] [a] J. Nasielski, A. Standaert, R. Nasielski-Hinkens, *Synth. Commun.* **1991**, 21, 901−906; [b] G. Vlád, I. T. Horváth, *J. Org. Chem.* **2002**, 67, 6550−6552.

[15] [a] A. Charisiadis, V. Nikolaou, K. Karikis, C. Giatagana, K. Chalepli, K. Ladomenou, S. Biswas, G. D. Sharma, A. G. Coutsolelos, *New J. Chem.* **2016**, 40(7), 5930–5941; [b] A. Brun, G. Etemad-Moghadam, *Synthesis* **2002**, 10, 1385–1390; [c] T. Nakanishi, N. Miyashita, T. Michinobu, Y.Wakayama, T. Tsuruoka, K. Ariga, D. G. Kurth, *J. Am. Chem. Soc*. **2006**, 128(19), 6328–6329; [d] T. Asghari, M. Bakavoli, M. Rahimizadeh, H. Eshghi, S. Saberi, A. Karimian, F. Hadizadeh, M. Ghandadi, *Chem. Bio.&amp ; Drug Design* **2014**, 85(2), 216–224.

[16] D. Ceylan-Erdoğan, E. Ahlatcıoğlu, Özerol, H. Ocak, B. Bilgin-Eran, *J. Mater. Sci. Mater. Electron.* **2021**, 32, 28870–2888.

[17] E. J. Corey, P. L. Fuchs, *Tetrahedron Lett*. **1972**, 3769–3772.

[18] J. Wolska, J. Mieczkowski, D. Pociecha, S. Buathong, B. Donnio, D. Guillon, E. Gorecka, *Macromolecules* **2009**, 42, 6375–6384.

[19] P. Nicolas, S. Abdallah, A. Dok, Y. de Coene, O. Jeannin, N. Bellec, J.-P. Malval, T. Verbiest, K. Clays, S. Van Cleuvenbergen, B. Bilgin-Eran, H. Akdas-Kiliç, F. Camerel, *Chem. Asian J.* 2024, e202400112.

[20] Savel, P., Akdas-Kilig, H., Malval, J.-P., Spangenberg, A., Roisnel, T., Fillaut, J.-L. *J. Mater. Chem.* C 2014, 2, 295-305.

[21] C. Lambert, E. Schmälzlin, K. Meerholz, C. Bräuchle, *Chem. Eur. J.* **1998**, 4, 512-521; F. Terenziani, C. Katan, E. Badaeva, S. Tretiak, M. Blanchard-Desce, *Adv. Mater*. **2008**, 20, 4641-4678; D. Beljonne, W. Wenseleers, E. Zojer, Z. Shuai, H. Vogel, S. J. K. Pond, J. W. Perry, S. R. Marder, J. L. Brédas, *Adv. Funct. Mater.* **2002**, 12, 631.

[22] U. Bora, S. Abdallah, R. Mhanna, P. Nicolas, A. Dok, Y. de Coene, S. Van Cleuvenbergen, O. Jeannin, J.-P. Malval, K. Clays, N. Bellec, H. Ocak, B. Bilgin-Eran, F. Camerel, H. Akdas-Kiliç, *Chem. Eur. J.* **2024**, 30, e202302930.

[23] R. Meech,D. J. Phillips, *J. Photochem.* **1983**, 23, 193–21

[24] D. V. Connor, D. Phillips, *Time correlated single photon counting,* **1984**, Academic Press, London.

[25] D. Lewis, R. S Kalgutkar, J.-S Yang, *J. Am.Chem.Soc*. **1999**, 121, 12045–12053.